CAMBRIDGE
UNIVERSITY PRESS

Research Paper

A survey of extended matter around chromospherically active binary systems

Osman Karakuş and Fehmi Ekmekçi [ORCID]

Faculty of Science, Department of Astronomy and Space Sciences, Ankara University, 06100 Tandoğan, Ankara, Turkey

Abstract

We present an analysis of colour excess *(CE)* observations for 13 chromospherically active binary systems, together with 27 inactive reference stars of similar spectral types and luminosity classes of the components of these 13 binaries. We used the observations which were made by Johnson-Cousins BVR_cI_c, *2MASS*, and *WISE* photometric systems. Our new photometric BVR_cI_c observations were obtained by means of 1 m telescope at TÜBİTAK National Observatory and 40 cm telescope at Ankara University Kreiken Observatory. To check the existence of extended matter around an active binary component(s) of these 13 binary systems, we examined the *CE* values at around primary/secondary minima and outside eclipses. The comparison of these *CEs*, obtained relative to those of reference stars of the same $(B - V)_\circ$ colours, especially during primary minima with those of secondary minima and outside eclipses, showed that these systems have greater excess radiation in primary minima than in both secondary minima and outside eclipses. We observed that the colour excesses, in general, most likely arise from the extended matter around the cooler component of a binary system. The comparison of *CE* values also showed that the extended matter of some of these systems was most likely covered or affected both of their components. Since no observational data were obtained during primary minimum of *RW UMa*, by excluding this binary system, an examination of the locations of cool and active components of the remaining 12 systems of this study on Hertzsprung-Russell diagram, together with corresponding evolutionary tracks, showed that most of the active binary systems have an extended matter not only caused from stellar activity but also more likely caused from evolutionary processes.

Keywords: stars: activity – (stars:) binaries: eclipsing – stars: chromospheres – (stars:) circumstellar matter – (stars:) Hertzsprung-Russell (HR) diagrams – (stars:) starspots

(Received 19 February 2019; revised 14 January 2020; accepted 15 February 2020)

1. Introduction

Chromospherically active binaries *(CABs)* are detached binary systems with cool components characterised by strong chromospheric, transition region, and coronal activity. Phenomena of the chromospheric activity are seen mostly in late-type stars, including RS CVn binaries and BY Dra variables. The current catalogue of *CABs*, as a third edition, was given by Eker et al. (2008). The RS CVn binaries have at least one cool evolved component, whereas both components of the BY Dra binaries are main sequence stars. Fekel, Moffet, & Henry (1986) indicate that chromospherically active stars have colour excesses (CEs) in $(V - R)$ and in $(V - I)$ by using their photometric observations of 52 late-type stars.

A survey for extended matter has been presented by Hall & Ramsey (1992) to determine the frequency and nature of circumstellar matter in these *CABs*. Hall & Ramsey (1992) have detected large regions of extended, prominence-like material, which has been shown to be a common feature in these systems. Extended material in the *CABs* is difficult to detect in emission, but if the same extended region occurs in an eclipsing star, it may obscure a large fraction of the eclipsed star's disk at phases near the outer contact points of the light curve and may produce a significant

absorption feature in the spectrum. When an extended region projected against the star disk appeared through the line of sight of an observer at a phase near the outer contact, some excess emission/absorption features may be discoverable. That is, such an extended region is more easily detected at a phase near the outer contact case (for well-illustrated figures, see Hall & Ramsey 1992, 1994). Although RS CVn- and BY Dra-type binaries were incorporated into a group after 1990s as *CABs* (see Strassmeier et al. 1988), which are a common group name for both RS CVn- and BY Dra-type stars, we also see that some BY Dra-type binaries exhibit similar IR excess, in infrared astronomical satellite (IRAS) bands, to those of RS CVn binaries (see Chugainov & Lovkaya 1989).

Busso et al. (1990) have studied the infrared (IR) emission of active binaries and they concluded that about 40% of RS CVn-type binary systems, studied up until then, exhibit IR excess. They also discussed the presence of thin circumstellar shells together with the evolutionary status of the binary components to give a possible explanation for this excess emission.

Montes et al. (1996) emphasised that 'The high levels of activity observed in the chromospherically active stars are generally attributed to the presence of deep convection zones and the fast rotation that drives the dynamo mechanism'. As a component of *CABs*, the stars are usually forced to rotate relatively rapidly due to tidal interactions and typically the rotation period is synchronised with the orbital period of the binary system (Montes et al. 1996).

Scaltriti et al. (1993) have analysed the energy distributions of 12 RS CVn-type binaries and they also confirmed that the circumstellar matter around CABs is clearly present. They also evaluated the mass of absorbing material which is supposed to be in the form of silicate grains. They suggested that the circumstellar envelopes are built by the integrated mass loss, which is fed by stellar winds driven by magnetic activity. By comparing the IR excess of the sources in these 12 binary systems, they speculated that the circumstellar envelopes are related to stellar activity phenomena of the RS CVn-type binary systems. The stellar activity definition based on photospheric, chromospheric, and coronal phenomena was given in detail by Rodonó (1980).

Assessments of the roots of the disk structure around CAB stars began with the IRAS in 1983. IRAS was the first mission to put a telescope in space to survey the All-sky survey at 12, 25, 60, and 100 micron bands.

On the other hand, Busso et al. (1988) also found in their study of RS CVn-type binaries, which is based on IRAS observations, that the IR excess is definitely present in CF Tuc, while the spectral distributions of the λ And, UX Ari, and AR Lac can be accounted for. They also concluded that the excess is not correlated with the activity level, nor with the evolutionary status, but may be correlated with the mass-loss phenomena (triggered by the binary nature?) near the Main Sequence (see Busso et al. 1988).

The aim of this study is to put forward the characteristics of the extended/circumstellar matter, that may be present in CAB systems, and then to search the relation between this matter and evolutionary status of the component stars, depending on stellar activity, by examining the locations of cooler components of *CABs* on the Hertzsprung-Russell *(HR)* diagram, with corresponding evolutionary tracks. Because the spectral types of the components of *CABs* are between (F2 IV-G V-IV) and M2 V (see Strassmeier et al. 1988; Eker et al. 2008). Therefore, the search of the activity level/IR excess (and therefore the investigation of extended/circumstellar matter), depending on the location of the components of *CABs* on the *HR* diagram, together with corresponding evolutionary tracks, may reveal an observational evidence that may be associated/correlated with evolution. Expectations of the presence of extended/circumstellar matter in *CABs*, as it can be seen from the summarisation of studies given above, can be based on the observational results that were previously found and listed below:

– presence of excess radiation at *UV* and *IR* spectral regions (e.g. Rhombs & Fix 1977; Busso et al. 1990; Scaltriti 1990; Scaltriti et al. 1993; Ekmekçi 2010),
– presence of flares (e.g. Simon, Linsky, & Schiffer 1980; Brown & Brown 2006),
– polarisation and radio observations (e.g. Mutel & Weisberg 1978; Mutel et al. 1987),
– IRAS observations (e.g. Busso et al. 1988; Mitrou et al. 1996).

That is, the detection of *CEs*, especially in IR spectral regions, clearly suggests that there is circumstellar material in the system (e.g. Scaltriti et al. 1993). The excess radiation at the UV spectral region provides observational evidence of stellar activity, while excess radiation at the IR spectral region provides observational evidence of extended/circumstellar matter. The other method to determine the existence of an extended/circumstellar matter in a binary system is to compare the spectral energy distribution (SED)

Table 1. List of programme stars selected for this study. CAB numbers were taken from the catalogue given by Eker et al. (2008)

CAB Num.	Name	Spectral type	Period (days)
55	LX Per	F8V + G8IV–V	8.04
118	SV Cam	F9V + K4V	0.59
120	VV Mon	K0IV + G2IV	6.05
145	GK Hya	F8V + G8IV	3.59
199	RW Uma	F9V + K1IV	7.33
219	UX Com	G2V + K1III –IV	3.64
223	RS CVn	F4IV + G9IV	4.80
251	SS Boo	G0V + K1IV	7.61
312	PW Her	K0IV + F8 –G2	2.88
314	AW Her	G2IV + K2IV	8.80
383	RT Lac	G9IV + K1IV	5.07
385	AR Lac	G2IV + K0IV	1.98
399	RT And	G0V + K2V	0.63

of an active system with the SED of a reference star of the same $(B - V)_\circ$ (see Figures 2 and 3).

In accordance with this purpose, 13 chromospherically active and total eclipsing binary systems, listed in Table 1, were selected and their photometric BVR_cI_c observations were made at TÜBİTAK National Observatory (TUG) and Ankara University Kreiken Observatory (AUKR) during the period 2012–2014. The Two Micron All-Sky Survey (2MASS) and Wide-field Infrared Survey Explorer (WISE) observations were also included in the photometric data obtained by using the TUG and AUKR telescopes. To search the CEs for these 13 eclipsing binaries, 27 single stars of the same spectral types and of the same luminosity classes with those of the components of these 13 binary systems were also included in the observation schedules. These 27 stars, used as reference stars in this study, are listed in Table 2. The observational results are presented below in Section 2.1.

2. Observations and data reductions

2.1. Photometric observations

We selected 13 chromospherically active and total eclipsing binary systems as programme stars. In addition, several inactive stars, as reference stars, of similar spectral types and luminosity classes with those of the components of these binary systems have also been observed. With the aim of investigation of photometric characteristics/effects of any extended matter around component(s) of these active binaries, we attempted to make BVR_cI_c observations during minima and outside eclipses.

Photometric observations of all stars, listed in Tables 1 and 2, in the Johnson-Cousins BVR_cI_c photometric system were obtained at TUG[a] 1 m (T100) telescope at Bakırltepe, Antalya, in Turkey and at AUKR[b] 40 cm (T40) telescope at Ankara, in Turkey from 2012 July to the end of 2014 August. Properties of photometric bands

Table 2. List of reference stars (inactive stars)

Name	Spectral type Simbad and (Ref.)	This study
HD 116044	G8IV D (–)	K2 III
HD 232843	K0III (Bouigue 1959)	K3 III
BD + 01 1945	G8IV (Chuadze 1973)	K3 III
HD 231848	K0III (Boulon 1963)	K3 III
HD 210925	K0IV (Harlan 1969)	K3 III
HD 292944	K5 (Nesterov et al. 1995)	K4 III
HD 131447	K0IV (Heard 1965)	K5 III–IV
HD 235751	G8IV (McCuskey 1955)	K6 III
BD + 28 2165	K1IV D (Upgren 1962)	K8 III
HD 127824	F4IV (Moore & Paddock 1950)	F5 IV
HD 336601	G0 (Nesterov et al. 1995)	F9 IV
HD 195405	G2IV (Bidelman 1957)	F9 IV
HD 18403	G0IV (Heard 1950)	G0 IV–V
HD 291029	G5 (Nesterov et al. 1995)	G1 IV
BD + 28 3198	G2V D (–)	G1 IV
BD + 26 3026	G8IV (Yoss 1961)	G9 IV
HD 111094	K0IV (Yoss 1961)	K3 IV
BD + 54 2777	K0IV (McCuskey 1955)	K4 IV
TYC 3973-2446-1	G5V D (–)	K5 IV
BD + 46 1042	F5V (Chuadze 1973)	F0 V
HD 95975	F7IV (Heard 1965)	F5 V
HD 216685	F8V D (–)	F6 V
HD 145404	G0V (–)	F9 V
HD 259516	G2V (Chuadze 1973)	G0 V
HD 111540	G1VD (–)	G1 V
HD 56168	K2.5V (Gray et al. 2003)	K2 V
HD 233357	K3V (Loth & Bidelman 1998)	K4 V

Table 3. Properties of photometric bands used in this study

Band	λ(pivot) (Angstrom)	Bandwidth (Angstrom)	Zero-magnitude fluxes (Janskys)	Reference
B	4 326	1 816	3 962	Pickles & Depagne (2010)
V	5 445	1 129	3 688	Pickles & Depagne (2010)
R_c	6 529	1 877	3 195	Pickles & Depagne (2010)
I_c	8 104	1 604	2 520	Pickles & Depagne (2010)
J	12 350	1 620	1 594(27.8)	Cohen, Wheaton, & Megeath (2003)
H	16 620	2 510	1 024(20.0)	Cohen et al. (2003)
K_s	21 590	2 620	666.8 (12.6)	Cohen et al. (2003)
W1	33 526	6 625.6	306.7(4.6)	Jarrett et al. (2011)
W2	46 028	10 423	170.7(2.6)	Jarrett et al. (2011)
W3	115 608	5 5069	29.0 (0.4)	Jarrett et al. (2011)
W4	220 883	41 013	8.28 (0.3)	Jarrett et al. (2011)

calibration coefficients of T100 and T40 telescopes given by Ak (2013) and Karakuş & Ekmekçi (2017), respectively. In order to estimate the nightly photometric zero points, Landolt's standard stars (Landolt 2009) were used (see Karakuş & Ekmekçi 2017). First-order extinction coefficients, k'_B, k'_V, k'_R, and k'_I, have the average values of 0.337 ± 0.119, 0.209 ± 0.088, 0.152 ± 0.069, and 0.101 ± 0.053 mag (obtained from 17 nights) for observations made at TUG and 0.413 ± 0.110, 0.239 ± 0.075, 0.174 ± 0.066, and 0.107 ± 0.057 mag (obtained from 43 observation nights) for observations made at AUKR, respectively.

The light elements used in this study for each binary system were taken from the website of *TIDAK (TIming DAtabase at Krakow)*[d]. For all 13 active binary systems of this study, the zero phase corresponds to conjunction with the cooler component in front.

2.2. 2MASS and WISE observations

2MASS[e] has covered the whole sky observations (see Skrutskie et al. 2006) in the bands J(1.25 μm), H(1.65 μm), and Ks (2.17 μm). The observational 2MASS data of all stars used in this study were taken from the All-Sky Point Source Catalog. The 2MASS data of 13 binaries and reference stars of this study, listed in Tables A.1 and A.2, have been obtained during the period 1997–2000. We were able to detect that only one scan was made for each of these stars during 2MASS observations.

The WISE[f] (see Wright et al. 2010) is a NASA mission that has mapped the sky which has four IR bands: W1 (3.4 μm) , W2 (4.6 μm), W3 (12 μm), and W4 (22 μm). Photometric data of reference stars and programme stars, obtained with these bands of WISE, were taken from All WISE Source Catalogue and All WISE Multiepoch Photometry Catalogue, respectively. WISE is achieving a sensitivity more than 100 times better than IRAS in the 12 μm band. All WISE data used in this study were obtained between 2010 January 7 and 2010 July 16 with a cryogenically cooled telescope.

Our photometric CCD observations were also evaluated together with the observations of multiepoch IR photometry of

used in this study are given in Table 3. The log of observations is given in Tables 4 and 5. The reduction of the CCD frames has been performed with aperture photometry using standard packages of IRAF[c].

The instrumental setup of the T100 telescope system of TUG contains an ACE RC 1.0, 1 m aperture *Ritchey-Chretien* telescope, *SI 1100, 4K X 4K* CCD camera, and Bessel *BVRI* filter set. The instrumental setup of the T40 telescope system of AUKR contains a *MEADE LX200-GPS* 16″ aperture Schmidt-Cassegrain reflecting telescope, an *APOGEE ALTA U47-MB 1024 X 1024* 13 μm pixels CCD camera, and Schüler Johnson-Cousins *BVRI* filter set.

Instrumental magnitudes were used to obtain the magnitudes outside of the atmosphere by using the first-order extinction coefficients for all observed nights. The average second-order extinction coefficients were derived from the calculations of the T100 telescope by Ak (2013) and of the T40 telescope by Karakuş & Ekmekçi (2017). Also, the instrumental magnitudes and colours were transformed to standard photometric systems by using the

---

[c]IRAF is distributed by the National Optical Astronomy Observatory, which is operated by the Association of Universities for Research in Astronomy, Inc., under cooperative agreement with the National Science Foundation.

[d]http://www.as.up.krakow.pl/ephem/
[e]http://irsa.ipac.caltech.edu/Missions/2mass.html
[f]http://irsa.ipac.caltech.edu/Missions/wise.html

Table 4. Log of CCD observations of chromospherically active binaries

		# of data for	rms errors			
System	Obs. dates	each colour	σ_{B-V}(mag)	σ_{V-R}(mag)	σ_{V-I}(mag)	σ_{R-I}(mag)
LX Per	Aug 25, Sep 22, 29, 2012;	950	0.054	0.035	0.035	0.033
	July 21, Aug 24, Sep 14, 21, Oct 11, 25,					
	Nov 01, 08, 2013; Mar 21, 2014					
SV Cam	Sep 08, 09, 2012	21	0.031	0.033	0.021	0.031
VV Mon	Nov 01, Dec 13, 2013; Jan 31, Feb 07, 2014	185	0.055	0.039	0.036	0.033
GK Hya	Jan 31, Feb 07, 2014	40	0.057	0.042	0.039	0.037
RW UMa	Dec 13, 2013; Jan 31, Feb 07, Mar 14, 2014	127	0.043	0.029	0.033	0.029
UX Com	May 25, 2013; Jan 31, Feb 07, Mar 14, 2014	127	0.052	0.038	0.036	0.032
RS CVn	Aug 24, 2012; Apr 13, 27, May 26, June 24,	105	0.058	0.043	0.046	0.042
	25, July 01, 02, 21, 2013					
SS Boo	Aug 31, Sep 30, 2012; Apr 27, June 23,	51	0.045	0.034	0.037	0.034
	July 01, 02, 20, 21, 2013					
PW Her	Aug 24, Sep 10, 30, Nov 03, 2012;	161	0.059	0.041	0.038	0.036
	June 01, 22, 23, 24, July 06, 26, Aug 24,					
	Sep 07, 14, 2013					
AW Her	Aug 24, 25, Sep 10, 29, 30, 2012;	160	0.053	0.038	0.039	0.036
	May 25, June 25, July 02, 06, 20, 21, 26,					
	Aug 25, 26, Sep 14, 2013					
RT Lac	July 20, Aug 24, 25, 30, Sep 09, 22, 29, 2012;	318	0.062	0.039	0.036	0.033
	June 25, July 02, 20, Aug 02, 03, 25, 26,					
	Sep 07, 14, 2013					
AR Lac	July 21, Aug 24, 25, Nov 03, 2012;	300	0.061	0.043	0.042	0.041
	June 22, 23, 24, July 01, 02, 06, 26, 2013					
RT And	July 20, 21, Aug 24, 25, 30, 31, Sep 22, 2012	293	0.048	0.029	0.032	0.029

WISE of these 13 programme stars by using all data depending on orbital phases. Thus, this study gave the first combination results with the multiepoch photometric data for these 13 chromospherically active and total eclipse binary stars.

2.3. De-reddening of magnitudes and the evaluation of colours

The interstellar medium has the effect of emission and absorption on the light of a star. This effect varies depending on the distances and galactic position of a star. The total interstellar absorption, $A_\infty(b)$, depending on BVR_cI_c bands could be estimated by using NED service[g] (see Schlafly & Finkbeiner 2011). By using the equation given by Bahcall & Soneira (1980), as written below, the total absorption at an infinite distance $[A_\infty(b)]$ was reduced to the $A_d(b)$ absorption of the star at distance d:

$$A_d(b) = A_\infty(b) \left[1 - exp \left(\frac{-\mid d \sin(b) \mid}{H} \right) \right]. \qquad (1)$$

Here, b and d are galactic latitude and distance of the star, respectively. H is the scale height for the interstellar dust. In this study, the value of H was adopted as 125 pc as considered in

Marshall et al. (2006) and the distances of stars are obtained from *Gaia*[h] *Data Release 2 (GAIA DR2)*.

Thus, the related $A_d(b)$ values for each star were calculated by using Equation (1), as given above. Also, in order to determine total absorptions (A_v values) in the bands of BVR_cI_c, 2MASS, and WISE photometric systems, we used the relations given by Cardelli, Clayton, & Mathis (1989).

After these reduction procedures, the colour-colour diagrams of programme stars at the primary minimum phases were obtained, and then the evaluations of these colours, together with the lines of linear correlation fits of reference stars, were obtained as shown in Figure 1. By applying the regression analysis to photometric CCD data of reference stars, we have the linear coefficients of colour-colour relations (as $y = a + bx$) as follows:

$$(V-R)_\circ = 0.034[\pm 0.015] + 0.487[\pm 0.018](B-V)_\circ$$
$$\text{with } r^2 = 0.967; \sigma_{CE(V-R)} = 0.026, \qquad (2)$$

$$(V-I)_\circ = 0.089[\pm 0.027] + 0.888[\pm 0.031](B-V)_\circ$$
$$\text{with } r^2 = 0.970; \sigma_{CE(V-I)} = 0.045, \qquad (3)$$

$$(R-I)_\circ = 0.053[\pm 0.014] + 0.404[\pm 0.016](B-V)_\circ$$
$$\text{with } r^2 = 0.961; \sigma_{CE(R-I)} = 0.024, \qquad (4)$$

Table 5. Log of CCD observations of reference (inactive) stars

System	Obs. dates	# of data for each colour	rms errors σ_{B-V} (mag)	σ_{V-R} (mag)	σ_{V-I} (mag)	σ_{R-I} (mag)
HD 116044	Aug 24, 2012; Apr 27, June 01, July 01, 21, 2013	30	0.016	0.008	0.008	0.009
HD 232843	Sep 22, 2012; Aug 24, Sep 14, 21, Oct 11, 25, Nov 01, 08, 2013; Aug 23, 2014	241	0.009	0.007	0.008	0.007
BD + 01 1945	Jan 31, Feb 07, 2014	15	0.009	0.008	0.014	0.013
HD 231848	Aug 24, Sep 10, 2012; June 22, 23, 24, July 21, 26, 2013; Aug 02, 2014	69	0.011	0.008	0.009	0.008
HD 210925	July 20, 21, Aug 24, 25, Nov 03, 2012; June 22, July 02, 26, Aug 24, Sep 14, 2013; June 13, 20, July 05, Aug 09, 23, 30, 2014	170	0.028	0.021	0.032	0.028
HD 292944	Oct 25, Nov 01, 2013; Jan 31, Feb 07, 2014	107	0.011	0.009	0.009	0.006
HD 131447	Aug 24, 31, Sep 30, 2012; Apr 27, June 01, 23, July 01, 2013; May 16, July 12, 2014	54	0.014	0.012	0.018	0.017
HD 235751	July 20, Aug 30, Sep 09, 22, 2012; July 20, Aug 02, 03, 25, 26, Sep 07, 14, 2013; June 13, Aug 09, 16, 23, 2014	169	0.016	0.008	0.011	0.008
BD + 28 2165	Jan 31, Feb 07, May 16, June 13, 2014	32	0.017	0.006	0.007	0.007
HD 127824	Apr 13, 27, May 26, June 01, July 01, 21, 2013; June 13, 20, July 12, 2014	74	0.011	0.008	0.009	0.008
HD 336601	Aug 24, 25, Sep 10, 2012; June 22, 23, 24, July 26, Aug 24, Sep 07, 2013; June 20, July 12, Aug 02, 2014	77	0.012	0.013	0.009	0.011
HD 195405	July 21, Aug 24, Sep 22, Nov 03, 2012; June 22, 23, 24, July 01, 02, 26, Aug 24, 2013; June 20, July 05, 2014	103	0.013	0.009	0.013	0.009
HD 18403	Aug 31, Sep 22, 2012; July 21, Aug 24, Sep 13, 14, 21, Oct 11, Nov 01, 08, 2013; Jan 31, Aug 23, 2014	153	0.038	0.008	0.009	0.006
HD 291029	Jan 31, Feb 07, 2014	19	0.011	0.009	0.011	0.009
BD + 28 3198	Aug 24, 30, Sep 10, 2012; May 25, June 25, July 20, 21, 26, Aug 25, 26, 2013; June 13, 20, 2014	105	0.014	0.009	0.016	0.012
BD + 26 3026	Aug 24, 25, 30, 2012; June 25, 26, July 20, 21, 26, Aug 25, 26, 2013; June 20, Aug 02, 2014	61	0.012	0.016	0.011	0.015
HD 111094	Feb 07, Mar 14, June 20, 2014	25	0.012	0.009	0.009	0.005
BD + 54 2777	July 20, Aug 24, 25, 31, Sep 22, 2012; Sep 14, 2013; Aug 16, 23, 30, 2014	79	0.019	0.009	0.008	0.009
TYC 3973-2446-1	July 20, Aug 25, Sep 10, 22, 29, 2012; July 20, Aug 02, 03, 25, 26, Sep 07, 14, 2013; Aug 09, 16, 23, 2014	134	0.026	0.011	0.019	0.019
BD + 46 1042	Sep 22, Nov 03, 2012; Oct 11, 25, Nov 01, Dec 13, 2013	89	0.008	0.008	0.009	0.006
HD 95975	May 25, 2013; Feb 07, Mar 14, May 16, 2014	71	0.008	0.006	0.009	0.008
HD 216685	July 20, 21, Aug 30, 31, Sep 08, 09, 10, 22, 2012; Sep 14, 2013; June 20, July 05, Aug 09, 16, 23, 30, 2014	138	0.013	0.008	0.019	0.016
HD 145404	Aug 24, 31, 2012; Apr 27, June 01, 23, July 01, 06, 2013; June 13, 2014	80	0.016	0.016	0.025	0.021
HD 259516	Sep 08, 09, 22, 2012	12	0.007	0.012	0.009	0.011
HD 111540	May 25, 2013; Jan 31, Feb 07, May 16, June 13, 2014	42	0.011	0.007	0.007	0.007
HD 56168	Sep 22, Nov 03, 2012; Oct 11, 25, Nov 01, Dec 13, 2013	86	0.015	0.015	0.016	0.009
HD 233357	Sep 08, 09, 22, 2012; Aug 23, 2014	18	0.022	0.004	0.009	0.009
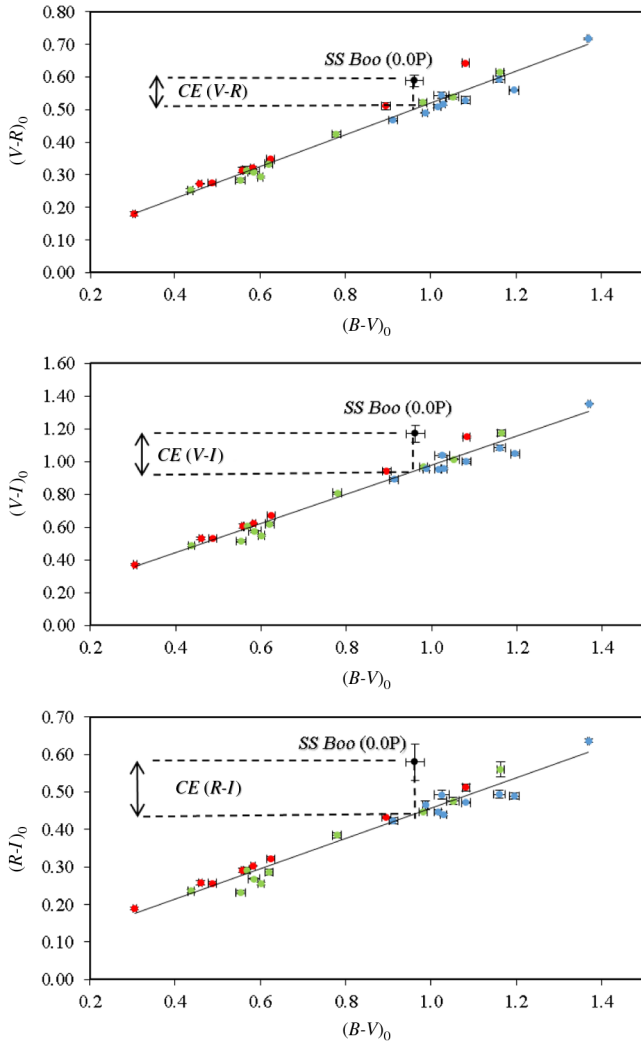
Figure 1. Three sample colour-colour graphs of linear correlation fits (straight lines) of reference stars, in $(V - R)$ (top panel), in $(V - I)$ (middle panel), and in $(R - I)$ (bottom panel). The colour-colour positions of programme star, SS Boo, at the primary minimum phases, were added to these diagrams as an explanation of the method we used for estimating their CE values. Reference stars of giant (III) are indicated as blue, of subgiants (IV) as green, and the main sequence stars (V) as red points, while programme star, SS Boo, is indicated black. Colours are in magnitudes.

$$(V - J)_\circ = 0.168[\pm 0.033] + 1.599[\pm 0.038](B - V)_\circ \tag{5}$$
$$\text{with } r^2 = 0.986; \sigma_{CE(V-J)} = 0.055,$$

$$(V - H)_\circ = 0.134[\pm 0.044] + 2.118[\pm 0.049](B - V)_\circ \tag{6}$$
$$\text{with } r^2 = 0.986; \sigma_{CE(V-H)} = 0.072,$$

$$(V - Ks)_\circ = 0.128[\pm 0.044] + 2.244[\pm 0.051](B - V)_\circ \tag{7}$$
$$\text{with } r^2 = 0.987; \sigma_{CE(V-Ks)} = 0.073,$$

$$(V - W1)_\circ = 0.177[\pm 0.049] + 2.256[\pm 0.057](B - V)_\circ \tag{8}$$
$$\text{with } r^2 = 0.984; \sigma_{CE(V-W1)} = 0.082,$$

$$(V - W2)_\circ = 0.108[\pm 0.057] + 2.301[\pm 0.066](B - V)_\circ \tag{9}$$
$$\text{with } r^2 = 0.979; \sigma_{CE(V-W2)} = 0.095,$$
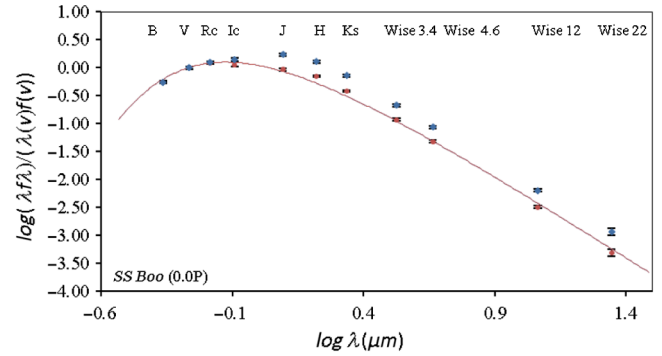
Figure 2. Comparison of SEDs of *SS Boo* and reference star *HD 111094*. The photometric values of *HD 111094* $[(B - V)_\circ = 0.98 \pm 0.01]$ are indicated as red points, while the values of *SS Boo* $[(B - V)_\circ = 0.96 \pm 0.02]$, during 0.0P, are indicated as blue points. The straight line shows the black body energy distribution of $T(K) = 4\,900$.

$$(V - W3)_\circ = 0.109[\pm 0.047] + 2.290[\pm 0.054](B - V)_\circ \tag{10}$$
$$\text{with } r^2 = 0.986; \sigma_{CE(V-W3)} = 0.077,$$

$$(V - W4)_\circ = 0.109[\pm 0.073] + 2.361[\pm 0.085](B - V)_\circ \tag{11}$$
$$\text{with } r^2 = 0.969; \sigma_{CE(V-W4)} = 0.122.$$

The colour versus $(B - V)_\circ$ diagrams obtained by using corresponding reference stars are constructed to determine the CE of programme stars. To find CE values of 13 binary systems of this study, we use the differences between the colours of binary stars and the colours obtained from colour-colour relations (Equations 2–11) with corresponding $(B - V)_\circ$ values (see Figures 1 and A.1). The rms values of related regression analysis were taken into consideration in the estimation of each CE value. The errors of CE magnitudes, as a measure of precision, were obtained by considering all absolute errors (i.e. nightly rms errors of each band observations and errors of parallaxes of stars from updated *Gaia* observations) in the relative error estimations. The CE values of the programme stars, as a function of orbital phase, are shown in Figures A.2, A.3, A.4, A.5, A.6, A.7, A.8, A.9, A.10, A.11, A.12, A.13, and A.14. The final photometric data of all stars are listed in Tables A.1 and A.2.

The normalised SEDs from visual-, near-, and mid-IR photometric data obtained during primary minima of some active binary systems (e.g. *SS Boo and UX Com*) were compared with SEDs of reference stars of the same $(B - V)_\circ$ (by using the approximation of a black body radiation) to reveal the excess (or residual) radiations in these systems (see Figures 2 and 3).

We have also reviewed the spectral types and luminosity classes for all selected stars using our photometric $(B - V)_\circ$ results. The spectral types which correspond to our $(B - V)_\circ$ results were attained from Sung et al. (2013) (see also column 3 of Table 2). Luminosity classes of these stars were determined by using the equation of M_v as

$$M_v = V_o - 5log(d) + 5 + A_d(b), \tag{12}$$

where d is *Gaia 2* distance of the star in parsecs. By using these values of M_v, the evolutionary status of all programme and reference stars is examined together with their positions on the HR diagram as shown in Figure A.17.
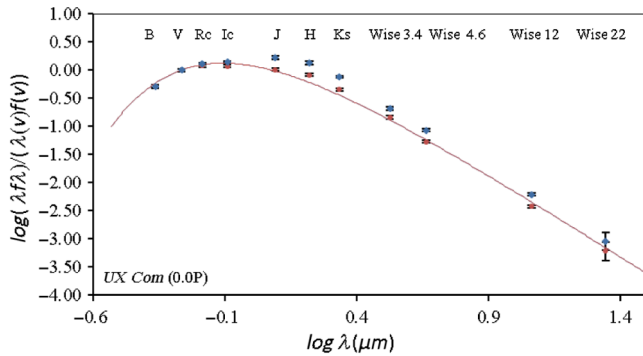
Figure 3. Comparison of SEDs of *UX Com* and reference star BD+54 2777. The photometric values of BD+54 2777 [$(B - V)_o = 1.05 \pm 0.012$] are indicated as red points, while the values of *UX Com* [$(B - V)_o = 1.04 \pm 0.04$], during 0.0P, are indicated as blue points. The straight line shows the black body energy distribution of $T(K) = 4\,700$.

2.4. CE as a function of wavelength

We also try to present a search for distribution of *CE* values depending on wavelength (in optical and in 3.4, 4.6, 12, and 22 μm bands) during minima and outside eclipses for 13 binary systems. Figure A.15 shows the CE of 13 programme stars of this study in all bands obtained during minima and outside eclipses. And, Figure A.16 shows the distributions of excesses as a function of $(B - V)_o$ for 13 programme stars together with related regression lines, during primary minima. During primary minima, these regression lines have slopes of

0.09 ± 0.04 in $CE(V - R)$ versus $(B - V)_o$,

0.19 ± 0.15 in $CE(V - I)$ versus $(B - V)_o$,

0.92 ± 0.53 in $CE(V - W1)$ versus $(B - V)_o$,

1.12 ± 0.36 in $CE(V - W2)$ versus $(B - V)_o$,

and

0.99 ± 0.56 in $CE(V - W3)$ versus $(B - V)_o$.

The same trends were seen at secondary minima and at outside eclipses but with lower slopes. These slopes clearly show that the amount of excess radiation of 13 binary systems of this study has greater values towards longer wavelength (from optical to middle IR bands).

The characteristics of achievement results are given in Section 3 and discussed in Section 4.

3. Results

To test the confidence range of the CE values obtained from our observations, we used the rms values given in Equations (2)–(11) in Section 2.3. Also, to check the existence of extended/circumstellar matter of an active binary component(s) of 13 binary systems of this study (see Table 1), we examined the *CE* values of these systems (see Table A.2) at around 0.0P, 0.25P/0.75P, and 0.5P orbital phases by comparing their colours with those of the same $(B - V)_o$ reference stars which were used in the regression analysis of colour-colour diagrams (see Figure 1). These *CE* values were calculated by using the colour differences between the colours of systems and the colours of reference stars of the same $(B - V)_o$ colours. Corresponding colours of the

same $(B - V)_o$ reference stars were estimated from the regression analysis of colour-colour diagrams. The characteristics of *CE* results obtained for 13 CAB systems of this study are summarised below (for the total observing nights of each binary system, see Table 4):

LX Per ($F8V + G8IV - V$) was observed for a total of 12 nights between 2012 and 2014. By comparing the colours of the system at around 0.0P and 0.5P with the colours of the same spectral-type reference stars, we determined the *CE* values as listed in Table A.2. From this table, it can be seen that the *CE*s of *LX Per*, at around 0.0P, were increasing towards longer wavelengths. The similar trend was detected at around 0.5P with the increasing *CE* values towards longer wavelengths. At outside eclipses, around 0.25P or 0.75P, the *LX Per* binary system has some variations of *CE* values depending on wavelength.

SV Cam ($F9V + K4V$) was observed for a total of 2 nights in 2012. From Table A.2, it is seen that *SV Cam* has sudden variations in *CE* values, at around 0.0P, depending on wavelength. But the *CE* values of the system, at around 0.5P and at outside eclipses, were increasing towards longer wavelengths.

VV Mon ($K0IV + G2IV$) was observed for a total of 4 nights between 2013 and 2014. *VV Mon* had sudden variations in *CE* values, at around 0.0P and at outside eclipses, in optical *V,R,I* bands. But, in the mid-IR region, *CE* values of the *VV Mon* system, at outside eclipses, showed a gradual increase towards longer wavelengths.

GK Hya ($F8V + G8IV$) was observed for a total of 2 nights in 2014. Unfortunately, the observations only included the data of the zero phase of the system. *GK Hya* had some fluctuations in *CE* values, at around 0.0P, in all bands (optical *V,R,I* and mid-IR bands).

RW UMa ($F9V + K1IV$) was observed for a total of 4 nights between 2013 and 2014. Unfortunately, we could not have photometric data at around 0.0P, due to bad weather conditions during observing times. But we obtained the data around 0.5P and at outside eclipse phases of the system. From Table A.2, it can be seen that *CE* values of *RW UMa*, at around 0.5P, were increasing towards longer wavelengths. At outside eclipses, the system also had the same characteristics of increasing *CE* values depending on wavelength.

UX Com ($G2V + K1III - IV$) was observed for a total of 4 nights between 2013 and 2014. *UX Com* had some remarkable *CE* values, at around 0.0P, in optical *V,R,I* bands, whereas the system showed small fluctuations around ~0.5 mag in *CE* values, at around 0.0P, in mid-IR bands. At around 0.5P, the system had some increase in *CE* values towards longer wavelengths in optical *V,R,I* bands. No data at outside eclipses of *UX Com* system were obtained.

RS CVn ($F4IV + G9IV$) was observed for a total of 9 nights between 2012 and 2013. *RS CVn* had some remarkable fluctuations in *CE* values, at around 0.0P, in optical *V,R,I* bands, while at around 0.5P, the system showed some lower fluctuation in *CE* values in optical *V,R,I* and mid-IR bands. At outside eclipses, the system also had the same characteristics of increasing *CE* values depending on wavelength.

SS Boo ($G0V + K1IV$) was observed for a total of 8 nights between 2012 and 2013. The *CE* values of *SS Boo*, at around 0.0P, were increasing towards longer wavelengths, while at around 0.5P had some significant increases in *CE* values towards longer wavelengths in optical *V,R,I* bands. At outside eclipses, the system had the same characteristics of *CE* values in mid-IR bands.

PW Her ($K0IV + F8 - G2$) was observed for a total of 13 nights between 2012 and 2013. From Table A.2, it can also be seen that *CE* values of *PW Her*, at around 0.0P, were increasing towards longer wavelengths in optical *V,R,I* bands. The similar trend in *CE* values was detected at around 0.5P in optical *V,R,I* and mid-IR bands. At outside eclipses, the system also had the same characteristics of increasing *CE* values depending on wavelength.

AW Her ($G2IV + K2IV$) was observed for a total of 15 nights between 2012 and 2013. *AW Her* had some detectable *CE* values, at around 0.0P and 0.5P, in optical *V,R,I* bands. At outside eclipses, the system also has the same characteristics of increasing *CE* values depending on wavelength.

RT Lac ($G9IV + K1IV$) was observed for a total of 16 nights between 2012 and 2014. *RT Lac* had some increase in *CE* values towards longer wavelengths at around 0.0P, in optical *V,R,I* bands, while at around 0.5P, the system had some detectable *CE* values in optical *V,R,I* and mid-IR bands. At outside eclipses, the system had similar trends in *CE* variation in optical *V,R,I* and mid-IR bands. From these *CE* values (see Table A.2), it is seen that the *CE* values of the *RT Lac* system show the variations with the colours at outside eclipses, which are similar to those during both of the minima phases.

AR Lac ($G2IV + K0IV$) was observed for a total of 11 nights between 2012 and 2013. *AR Lac* had some fluctuations in *CE* values, at around 0.0P, at all bands used in this study. But the system shows some characteristic variations in *CE* values towards longer wavelengths at both around 0.5P and outside eclipse phases, while at outside eclipses, *AR Lac* had lower and some detectable *CE* values in all bands used in this study.

RT And ($G0V + K2V$) was observed for a total of 7 nights in 2012. *RT And* had some detectable *CE* values, at around 0.0P and 0.5P in all bands used in this study. At outside eclipses, the system had similar characteristics in *CE* values obtained from all bands used in this study.

4. Discussion and conclusions

For the purpose of this study, our BVR_cI_c photometric CCD observation data were obtained only during minima and outside eclipse phases of 13 chromospherically active total eclipsing binary systems we selected. Thus, it was attempted to evaluate both the contributions of the components of each binary system and *CE* measurements of a binary system that contribute to observed *CE* values, including total contributions of both components as a system. In order to investigate the existence and characteristics of possible extended/circumstellar matter in RS CVn-type binaries, we tried to evaluate our new Johnson-Cousins BVR_cI_c photometric CCD observations together with the near-IR JHK_s *(2MASS)* and mid-IR W1, W2, W3, and W4 *(WISE)* broadband photometric data of 13 chromospherically active total eclipsing binary systems. By comparing the colour indexes of 13 binary systems with those of corresponding nonactive reference stars, it can be seen that the CEs of these active binary systems (with a constant offset of $CE > 0$ mag; see Figures A.2, A.3, A.4, A.5, A.6, A.7, A.8, A.9, A.10, A.11, A.12, A.13, A.14, and A.15) could be attributed to existence and characteristics of possible extended/circumstellar materials located around one or both of the component(s). There are three phenomena that can cause this excess radiation in CAB systems:

(i) Existing cool spot(s) on the surface of an active star component,

(ii) Existing hot circumstellar gas in the system (e.g. Rhombs & Fix 1977), together with the effects of magnetic fields in the atmospheres of an active star component, and

(iii) Presence of a possible circumstellar disk/matter in the active binary system.

The best way to determine which of these phenomena may be in CABs is to find out whether these excess radiations are phase-dependent or not, and whether the excess radiation has variations depending on the phase or not. In addition, the excess radiation to be found by comparing the SED during primary/secondary minima of active binary system, with the SED of a reference star of the same $(B - V)_o$, provides evidence of the presence of a circumstellar disk/matter in this active binary system.

For example, an observed *CE* value of 0.25 mag in $(V - R)$ corresponds to an increase in the radiation flux of *R* band by 20%. This increase in radiation flux at longer wavelengths gives us a larger contribution from a possible extended/circumstellar matter in a binary system (e.g. an observed *CE* value of about 0.8 mag in $(V - W3)$ corresponds to an increase in the radiation flux of *W3* band by about 52%). The fact is that the larger *CE* values in the longer wavelengths of the spectral regions give us more precise observational evidence of the presence of extended/circumstellar matter in a binary system. For each binary system examined in this study, estimations about these flux contribution rates can be made by looking at the graphs given in Figure A.15.

Conclusions can be discussed as follows:

By examining the patterns of *LX Per*, given in Figure A.2, it can be seen that there may exist a small amount of *CE* independent of the orbital phase in the *LX Per* binary system. The comparison of *CE* levels of the system at about 0.0P with the levels of 0.5P and of the outside eclipses shows that there is some optical excess of about 0.04 mag and some near-IR excess of about 0.25 mag during secondary minimum in the *LX Per* binary system. Although there was a slight increase in *CE* values during the secondary minimum, there is almost no variation in *CE* values of the system, depending on orbital phases (see Figure A.2. Also, the comparison of *CE* levels in all bands during the minima and outside eclipses (see Figure A.15) shows that there is noticeable excess in the *LX Per* binary system. On the other hand, *LX Per* has *CE* values, at secondary minima phases, about 0.25 ± 0.02 in 2MASS bands and at outside eclipse phases, about 0.29 ± 0.03 in WISE bands (see Table A.2). Therefore, with these characteristics of *CE* levels, it can be concluded that the source of the excess in *LX Per* resulted mostly from the cooler component of the system. Hall & Ramsey (1992) denoted that excess emission of the *LX Per* binary system, obtained from their 1990 spectral observations, could probably have arisen from the chromospheres rather than the circumstellar environment. Our *CE* results of the *LX Per* binary system, obtained at all phases, are inconsistent with the results of Hall & Ramsey (1992). Based on the CE values of the *LX Per* active binary system in 2MASS and WISE bands obtained at all phases, it can be concluded that the extended/circumstellar matter could possibly be present in the system.

SV Cam is a short period, single-lined spectroscopic binary system ($F9V + K4V$, $P = 0^d.59$). The light curve shape of the system has variations as much as 0.1 mag during a month (Kjurkchieva, Marchev, & Ogłoza 2000). Busso et al. (1990) have not detected

an IR excess in the *SV Cam* binary system. This result may correspond to *J* band data as we found a decrease in the *CE* value of 0.07 mag in ($V - J$). Aside from this result, the *SV Cam* binary system had some significant values of *CE* at other wavelength ranges. The *SV Cam* has noticeable *CE* values of about 0.09 mag in optical spectral ranges (see Figure A.3) and *CE* values of about 0.1 mag in near-IR spectral ranges (see Table A.2) at about 0.0P. There is also a variation in *CE* values of *SV Cam*, depending on orbital phases. From a review of *CE* values in all bands as shown in Figure A.15, it is also seen that the main contribution to IR excess comes mostly from the cooler component of the *SV Cam* binary system. Şenavcı et al. (2013) found that the *SV Cam* shows excess emissions in CaII IR triplet lines through all orbital phases and this excess emission resulted from chromospheric active regions associated with star-spots. When all these features are evaluated together with the graph of *SV Cam* given in Figure A.15, it is seen that this active binary system may have an extended/circumstellar matter with a small probability.

VV Mon has remarkable *CE* values of about 0.15 mag in optical spectral ranges at about 0.1P, 0.9P, and 1.0P orbital phases (see Figure A.4). No observation was made in the near- and middle-IR spectral ranges during primary minimum of the *VV Mon* binary system. Since we could not have observational *V,R,I, 2MASS, and WISE* data during 0.5P orbital phases, we do not have corresponding *CE* values of *VV Mon* taken during a secondary minimum. But we have 2MASS and WISE data taken during outside eclipses for the *VV Mon* binary system (see Figure A.15). From this 2MASS and WISE data, it can also be seen that there are significant *CE* values in these bands at the outside eclipses in the *VV Mon* binary system. Based on the observed characteristic trends of *CE* values seen in other binary systems of this study (see Figure A.15), it may be inferred that the IR excess comes mainly from the cooler component of the *VV Mon* binary system. Busso et al. (1990) denoted that there is an IR excess in *VV Mon*. Together with all these characteristics, it can be seen that there is some certain observational evidence of extended/circumstellar matter in the *VV Mon* active binary system.

GK Hya has *CE* values in a low level of about 0.05 mag in the optical spectral ranges between 0.9P and 1.0P orbital phases (see Figure A.5). Unfortunately, we do not have any IR data at other orbital phases from our observations, nor 2MASS/WISE observations. However, an evaluation together with WISE data taken during primary minima of this binary system (see Figure A.15 and Table A.2) shows that the *GK Hya* binary system may have an IR excess level as low as 0.06 mag in $V - W3$ and this excess emission may come mainly from the cooler component of the *GK Hya* binary system. As can be seen from Figure A.15, there is no observational evidence for the presence of extended/circumstellar matter in the *GK Hya* active binary system.

Unfortunately, we could not collect any *CE* data during primary minimum of *RW UMa* from our observations nor 2MASS/WISE observations. Fortunately, during secondary minimum and outside eclipses of this system, we could take some *CE* measurements from our observations and 2MASS/WISE observations (see Figure A.6 and Table A.2). From these *CE* data, obtained at secondary minimum and at outside eclipses, we see that there is some excess emission in the *RW UMa* binary system in optical spectral ranges with the level of about 0.08 mag. In the near- and middle-IR spectral ranges, the system also has some definite *CE* values during secondary minimum and outside eclipses, which can be taken into consideration as evidence for excess emission.

This excess emission most probably comes from both components of *RW UMa* ($F9V + K1IV$), which can be attributed to chromospheric activity phenomena. Busso et al. (1990) and Scaltriti et al. (1993) reported that they did not detect an IR excess in the *RW UMa* binary system based on their 1986 and 1987 *IR* observations. Although we have no observational *CE* data at primary minimum for the *RW UMa* binary system, our *CE* measurements at secondary minimum and at outside eclipse phases suggest that there may be an observational evidence of a possible presence of some extended/circumstellar matter with some definite *CE* levels in this active binary system (see Figures A.6 and A.15).

From Figures A.7 and A.15, it can be seen that *UX Com* has definite *CE* values at a level of about 0.1 mag during both minima in optical spectral regions. The similar trend was seen in 2MASS and WISE data but with large errors (as large as 0.42 mag) in ($V - W4$) bandwidths. From the data with better level of errors, we see that *UX Com* has *CE* values of ∼0.49 mag in near-IR and of ∼0.46 mag in middle-IR spectral regions during primary minimum. By excluding the WISE observation, which has an error as large as 0.42 mag (corresponds to *CE* levels of 0.29 mag in ($V - W4$) bandwidths, see Table A.2), from observed *CE* levels, it can be concluded that the source of the excess in *UX Com* resulted mainly from the cooler component but with some contributions from its hotter companion of the system. Despite these high levels of uncertainty in *CE* measurements, these results suggest that there may be a structure in the *UX Com* binary system that provides some certain observational evidence of an extended/circumstellar matter (see Figures A.7 and A.15).

RS CVn has remarkable *CE* values of about ≥ 0.15 mag in optical spectral ranges at about primary minimum (see Figure A.8). No observation was made in the near- and middle-IR spectral ranges during primary minimum of the *RS CVn* binary system. The system also has some remarkable *CE* values of about 0.09 mag in optical spectral ranges during both of the secondary minimum and outside eclipses. And fortunately, there are 2MASS and WISE observations of this system during the secondary minimum and outside eclipses (see Table A.2 and Figure A.15). From these 2MASS and WISE data, it can also be seen that there are remarkable *CE* values in the near- and middle-IR spectral regions during both of the secondary minimum and outside eclipses in the *RS CVn* binary system. Based on the observed characteristic trends of *CE* values seen in the *RS CVn* binary system, it may also be referred that these excess emissions come mainly from the cooler component of this system. However, Berriman et al. (1983) have not detected an IR excess in the *RS CVn* binary system. As can be seen from the graph of *RS CVn* given in Figure A.15, there is definite observational evidence of the presence of an extended/circumstellar matter in this active binary system.

SS Boo, similar to *RS CVn*, has remarkable *CE* values of about ≥ 0.15 mag in optical spectral ranges at about primary minimum (see Figure A.9). This system has *CE* values of about ∼0.63 mag in both the near- and middle-IR spectral ranges at about primary minimum. Similarly with the *RS CVn* system, *SS Boo* also has some significant, but lower *CE* values in optical spectral ranges during secondary minimum (see Table A.2). There are only WISE observations during outside eclipses of *SS Boo*, but no 2MASS and WISE observations were made during secondary minimum of this system. Based on the observed characteristic trends of *CE* values seen in the *SS Boo* binary system, it may also be inferred that these excess emissions come mainly from the cooler component of this

system. The results of *CE* measurements of the *SS Boo* binary system shown in Figures 2 and A.15 provide certain observational evidence of extended/circumstellar matter in this active binary system.

PW Her has definite *CE* values at a level of about 0.1 mag during both minima in optical spectral regions (see Figure A.10). No observation was made in the near- and middle-IR spectral ranges during primary minimum of the *PW Her* binary system. The system also had some *CE* values in the range of about ∼ 0.1 mag in optical spectral ranges during both the secondary minimum and outside eclipses. Fortunately, there were 2MASS and WISE observations during secondary minimum of *PW Her* which gave us some definite *CE* values of about 0.2 mag in near-IR and of about 0.4 mag in middle-IR spectral ranges. With this characteristic level of *CE* values, it can be concluded that excess emissions come mainly from the cooler component of the *PW Her* binary system. From the graph of the *PW Her* binary system shown in Figure A.15, it is likely that this binary system, although not certain, seems to have observational evidence of an extended/circumstellar matter.

Similarly as in the *LX Per* system, *AW Her* has *CE* values as low as of ∼0.04 mag with high errors of ∼0.03 mag during primary minimum in optical spectral ranges (see Figure A.11). Our optical observations during secondary and outside eclipses of *AW Her* also gave *CE* values as low as of ∼0.04 mag with similar high errors as of primary minimum. No observation was made in the near- and middle-IR spectral ranges during primary and secondary minima of the *AW Her* binary system. The near-IR observations gave *CE* values of ∼0.19 ± 0.05 mag, while middle-IR observations gave *CE* values of ∼0.29 ± 0.03 mag during outside eclipses of the *AW Her* binary system. Based on these near-IR and middle-IR observations, which have higher accuracy than our optic observations, it can be concluded that there is some detectable excess emissions which probably come from the cooler component of the *AW Her* binary system. Based on their spectral observations taken in 1990 during primary eclipse of this system, Hall & Ramsey (1994) have concluded that *AW Her* shows evidence of an extended material. From the graph of the *AW Her* binary system shown in Figure A.15, we can see that our results support the results obtained by Hall & Ramsey (1994). It is also remarkable that it is similar to the *LX Per* binary system in terms of observational evidence of extended/circumstellar matter in this active binary system.

RT Lac has *CE* values of about 0.08 mag in optical spectral ranges at about primary minimum (see Figure A.12). No observation was made in the near- and middle-IR spectral ranges during primary minimum of the *RT Lac* binary system. The system also had some detectable *CE* values of about ∼0.05 and ∼0.07 mag in optical spectral ranges during secondary minimum and outside eclipses, respectively. No observation was made in the near-IR during secondary minimum of the *RT Lac* binary system. But there are 2MASS and WISE observations of this system during outside eclipses (see Table A.2 and Figure A.15). Based on all obtained *CE* values given in Table A.2, it can be concluded that the *RT Lac* binary system might have some excess emissions that mainly come from the cooler component of this system. This active binary system also has similarities with the *LX Per* system in terms of observational evidence of extended/circumstellar matter (see Figure A.15). That is, it can be concluded that the

extended/circumstellar matter could possibly, but uncertainly, be present in the *RT Lac* active binary system.

The *AR Lac* binary system had *CE* values as low as of ∼0.02 mag with high errors of ∼0.03 mag during primary minimum in optical spectral ranges (see Figure A.13). Our optical observations during secondary minimum of *AR Lac* also gave *CE* values as low as of ∼0.04 ± 0.02 mag while ∼0.01 ± 0.03 mag during outside eclipses. No observation was made in the near-IR spectral ranges during outside eclipses of the *AR Lac* binary system. The middle-IR observations gave *CE* values of ∼0.02 mag during primary minimum of the *AR Lac* binary system. A comparison of *CE* levels in all bands during the minima and outside eclipses (see Figure A.15) shows that there is noticeable excess only in ($V - W3$) bandwiths in the *AR Lac* binary system. Therefore, with these characteristics of *CE* levels, it can be concluded that the source of the excess in *AR Lac* resulted mostly from the cooler component of the system. Berriman et al. (1983) and Busso et al. (1990) have not detected an IR excess in the *AR Lac* binary system. By using the *Spitzer Space Telescope* data obtained between 2005 November and 2007 January, Matranga et al. (2010) have not detected a significant IR excess in the *AR Lac* binary system. But here, it should be noted that the WISE data have better sensitivity than of both IRAS and *Spitzer* data (see Wright et al. 2010). As can be seen from the graphs shown in Figures A.13 and A.15, there is no observational evidence that extended/circumstellar matter may exist in the *AR Lac* active binary system. In this system, the main source of excess radiation is stellar activity.

RT And had *CE* values of about 0.06 mag in optical spectral ranges at about primary minimum (see Figure A.14). No observation was made in the near- and middle-IR spectral ranges during primary minimum of the *RT And* binary system. But the observations made by WISE gave *CE* values of about ∼0.22 mag at about primary minimum. The system also had some detectable *CE* values of about ∼0.03 and ∼0.04 mag in optical spectral ranges during secondary minimum and outside eclipses, respectively. No observation was made in the near-IR during outside eclipses of the *RT And* binary system. A comparison of *CE* levels in all bands during the minima and outside eclipses (see Figure A.15) shows that there is noticeable excess in the *RT And* binary system. Therefore, with these characteristics of *CE* levels, it can be concluded that the source of the excess in *RT And* probably resulted from the cooler component of the system. There was no observational evidence for the presence of extended/circumstellar matter in the *RT And* active binary system either (see Figures A.14 and A.15). In this system, also, it is seen that excess radiations are caused by stellar activity.

Some characteristics of the evaluation of all *CE* measurements of 13 binary systems of this study can be summarised as follows:

– Our optical CCD observations of 13 CAB systems were obtained between 2012 and 2014. With the aim of investigating characteristics/effects of any extended matter around component(s) of a system, these observations of 13 binaries were attempted to be made during minima and outside eclipses. Fortunately, we were able to detect that only one scan made for each of the stars of this study during 2MASS observations was carried out between 1997 and 2000. We also found the WISE data of these stars obtained in 2010 with the full cooling systems of the satellite. The *CE* measurements from these 2MASS and WISE observations are consistent with those of our CCD observations (see Table A.2).

- The *SV Cam, RS CVn, SS Boo*, and *PW Her* binary systems showed *CE* variations in optical spectral ranges, depending on orbital phases, while the *LX Per, VV Mon, RW UMa, UX Com, AW Her*, and *RT Lac* binary systems did not show these types of *CE* variations as a function of orbital phases. However, the *AR Lac* and *RT And* binary systems were likely to have some *CE* variations depending on orbital phases. No enough photometric data were obtained to see this *CE* variation in *GK Hya*.

- Since the colour variations in optical filters are more sensitive to spot activity, the *CE* variations in these bands were attributed to stellar activity (Busso et al. 1987). Except for cases in *SV Cam* and *RT And* sytems, since the larger and cooler component is located in front of the hotter component and *CE* values at primary minimum are larger than that of the other orbital phases in the IR spectral ranges, the distributions shown in Figure A.16 provide some excess emission, which could be attributed to the presence of an extended/circumstellar matter around the cooler/primary component of the system.

- The active binary systems which show *CE* variations depending on orbital phases in optical spectral ranges may have some additional effects by about 0.03 mag in $(V - R)$, due to star spots (with a large spot area of 30% of the visible hemisphere and $\Delta T = 1\,000$ K) as reported by Fekel et al. (1986).

- In general, the amount of excess radiation of these 13 binary systems had greater values towards longer wavelengths (from optical to IR bands, see Figures A.15 and A.16). The excess radiation was detected in all orbital phases (in the minima and at the outside of minima) of these systems. *GK Hya* had an excess emission during primary minimum in optical spectral regions, but this system showed an absorption feature in *WISE* spectral regions during primary minimum. *GK Hya* also had excess emissions in *2MASS* and *WISE* spectral ranges during outside eclipses. It can be clearly seen from Figure A.15 that there are some increasing trends from relatively small *CE* values in optical *V,R,I* bands towards relatively larger *CE* values in middle-IR bands. This trend is to show that the excess in optical spectral ranges comes dominantly from the active component(s) of the system and towards the middle-IR spectral ranges, there are additional contributions due to heating the circumstellar matter around the active component(s). Therefore, the increase in *CE* values towards IR bands must be due to extended matter around active binary component(s) of an active binary system. Having clear excesses, at all phases and all bands, of some active binary stars of this study provided clear evidence of some hot and extended matter around cooler or both components of these systems.

- By comparing the excess radiation of these systems in primary minima with those of outside eclipses, we see that the systems have greater excess radiation in primary minimum than at outside eclipses. This trend may arise from the extended matter around the cooler component of a binary system.

- Amount of excess emission of a system may also provide information about the density of the gas around the system, showing the presence of a thin extended matter in the active binary system. The existence of a *CE* at *W3* (12 μm) could provide evidence for Silicate emission of an extended/circumstellar matter. From Table A.2, it can be seen that *CE* values, at $(V - W3)$,

for almost all 13 binaries of this study gave some evidence for Silicate emission (see Li, Zhao, & Li 2007; van Breemen et al. 2011) of an extended matter in these systems.

- Our results on measurements of excess emissions (obtained as *CE* values) in 13 binaries of this study were in agreement with the results of Busso et al. (1987) and Scaltriti (1990). They concluded that the IR spectral region proved to be a useful tool for study of IR emission, including *VV Mon*, from circumstellar matter which is formed in the expanding circumstellar envelopes as indicated by the case of *W Hyd*, which gave a large circumstellar dust shell around the red giant star (e.g. Hawkins 1990).

- According to our *CE* measurement results, the observational evidence regarding the extended/circumstellar matter is as follows:

  (a) Active binary systems without observational evidence of the presence of extended/circumstellar matter are *GK Hya, AR Lac, and RT And*,

  (b) Active binary systems with probable, but uncertain observational evidence of the presence of extended/circumstellar matter are *LX Per, SV Cam, PW Her, AW Her, and RT Lac*,

  (c) Active binary systems with certain observational evidence of the presence of extended/circumstellar matter are *VV Mon, RW UMa, UX Com, RS CVn, and SS Boo*.

- An examination of the locations of cooler components of 12 systems, with the exception of *RW UMa*, on the HR diagram (see Figure A.17) with corresponding evolutionary tracks (with solar *z* value of 0.02; see Lejeune & Schaerer 2001) shows that the stars of greater $(B - V)_{\circ}$ have greater *CE* values. Therefore, it can be concluded that most of the active components of binary systems might have an extended matter, caused not only from stellar activity but also more likely from evolutionary processes (see De Loore & Doom 1992; Iben & Livio 1993). The zero-age main sequence data we used in Figure A.17 were taken from Sung et al. (2013). For the location of these cooler components of 12 programme stars on the HR diagram in Figure A.17, we used the related $(B - V)_{\circ}$ and M_V as given in Tables A.2 and A.3, respectively.

- Based on our $(B - V)_{\circ}$ measurements (see Table A.1), the spectral types of reference stars which were used in this study have been updated as given in column 3 of Table 2.

References

Ak, T. 2013, TÜBİTAK National Observatory (TUG), unpublished

Bahcall, J. N., & Soneira, R. M. 1980, ApJS, 44, 73

Berriman, G., De Campli, W. M., Wermer, M. W., & Hatchett, S. P. 1983, MNRAS, 205, 859

Bevington, P. R. 1969, Data Reduction and Error Analysis for The Physical Sciences (New York: McGraw-Hill), 46

Bidelman, W. P. 1957, PASP, 69, 147

Brown, J. M., & Brown, A. 2006, ApJ, 638, L37

Bouigue, M. R. 1959, POHP, 4, 52

Boulon, J. 1963, POHP, 6, 45

Busso, M., Scaltriti, F., Persi, M., Robberto, M., & Silvestro, G. 1987, A&A, 183, 83

Busso, M., Scaltriti, F., Persi, M., Ferrari-Toniolo, M., & Origlia, L. 1988, MNRAS, 234, 445

Busso, M., Scaltriti, F., Ferrari-Toniolo, M., Origlia, L., Persi, P., Robberto, M., & Silvestro, G. 1990, MmSAI, 61, 77

Cardelli, J. A., Clayton, G. C., & Mathis, J. S. 1989, ApJ, 345, 245

Chuadze, A. D. 1973, AbaOB, 44, 105

Chugainov, P. F., & Lovkaya, M. N. 1989, Astrophysics, 30, 144

Cohen, M., Wheaton, W. A., & Megeath, S. T. 2003, AJ, 126, 1090

De Loore, C. W. H., & Doom, C. 1992, Structure and Evolution of Single and Binary Stars (Dordreccht/Boston/London: Kluwer Academic Publishers), 310–399

Eker, Z., et al. 2008, MNRAS, 389, 1722

Ekmekçi, F. 2010, PASA, 27, 1

Fekel F. G., Moffet, T. J., & Henry, G. G. 1986, ApJS, 60, 551

Gray, R.O. et al. 2003, AJ, 126, 2048

Hall, J. C., & Ramsey, L. W. 1992, AJ, 104, 1942

Hall, J. C., & Ramsey, L. W. 1994, AJ, 107, 1149

Harlan, E. A. 1969, AJ, 74, 916

Hawkins, G. W. 1990, A&A, 229L, 5

Heard, J. F. 1950, PDDO, 2, 105

Heard, J. F. 1965, PDDO, 2, 443

Iben, I. Jr, & Livio, M. 1993, PASP, 105, 1373

Jarrett, T. H., Cohen, M., Masci, F., et al. 2011, ApJ, 735, 112

Karakuş, O., & Ekmekçi, F. 2017, Ap&SS, 362, 116

Kjurkchieva, D., Marchev, D., & Ogłoza, W. 2000, AcA, 50, 517

Landolt, A. U. 2009, AJ, 137, 4186

Loth, A. L., & Bidelman, W. P. 1998, PASP, 110, 268

Lejeune, T. & Schaerer, D. 2001, A&A, 366, 538

Li, M. P., Zhao, G., & Li, A. 2007, MNRAS, 382L, 26

Marshall, D. J, Robin, A. C., Reylé, C., Schultheis, M., & Picaud, S. 2006, A&A, 453, 635

Matranga, M., Drake, J. J., Kashyap, V. L., Marengo, M., & Kuchner, M. J. 2010, ApJ, 720, L164

McCuskey, S. W. 1955, ApJS, 2, 75

Mitrou, C. K., Doyle, J. G., Mathioudakis, M., & Antonopoulou, E. 1996, A&AS, 115, 61

Montes, D., Fernández-Figueroa, M. J., Cornide, M., & De Castro, E. 1996, A&A, 312, 221

Moore, J. H., & Paddock, G. F. 1950, ApJ, 112, 48

Mutel, R. L., & Weisberg, J. M. 1978, AJ, 83, 1499

Mutel, R. L., Morris, D. H., Doiron, D. J., & Lestrade, J. F. 1987, AJ, 93, 1220

Nesterov, V. V., Kuzmin, A. V., Ashimbaeva, N. T., et al. 1995, A&AS, 110, 367

Pickles, A., & Depagne, É. 2010, PASP, 122, 1437

Rhombs, C. G., & Fix, J. D. 1977, ApJ, 216, 503

Rodonó, M. 1980, MmSAI, 51, 623

Scaltriti, F. 1990, in, Active Close Binaries, ed. C. İbanoğlu, NATO ASI Series (Vol. 319; Dordrecht/Boston/London, Kluwer Academic Publishers), 493

Scaltriti, F., Busso, M., Ferrari-Toniolo, M., Origlia, L., Persi, P., Robberto, M., & Silvetsro, G. 1993, MNRAS, 264, 5

Simon, T., Linsky, J. L., & Schiffer, F. H. 1980, ApJ, 239, 911

Schlafly, E. F., & Fingbeiner, D. P. 2011, ApJ, 737, 103

Skrutskie, M. F., Cutri, R. M., Stiening, R., et al. 2006, AJ, 131, 1163

Strassmeier, K. G., Hall, D. S., Zeilik, M., et al. 1988, A&AS, 72, 291

Sung, H., Lim, B., Bessel, M. S., et al. 2013, JKoAS, 46, 103

Şenavcı, H. V., Bahar, E., Montes, D., et al. 2018, MNRAS, 479, 875

Tümer, O., Ibanoğlu, C., Evren, S., & Tunca, Z. 1985, Ap&SS, 112, 273

Upgren, A. R. 1962, AJ, 67, 37

van Breemen, J. M., Min, M., Chiar, J. E., et al. 2011, A&A, 526A, 152

Weiler, E. J. 1974, PASP, 86, 56

Wright, E. L., Eisenhardt, P. R. M., & Mainzer, A. K. et al. 2010, AJ, 140, 1868

Yoss, K. M. 1961, ApJ, 134, 809

Appendix A. Some extra figures and tables
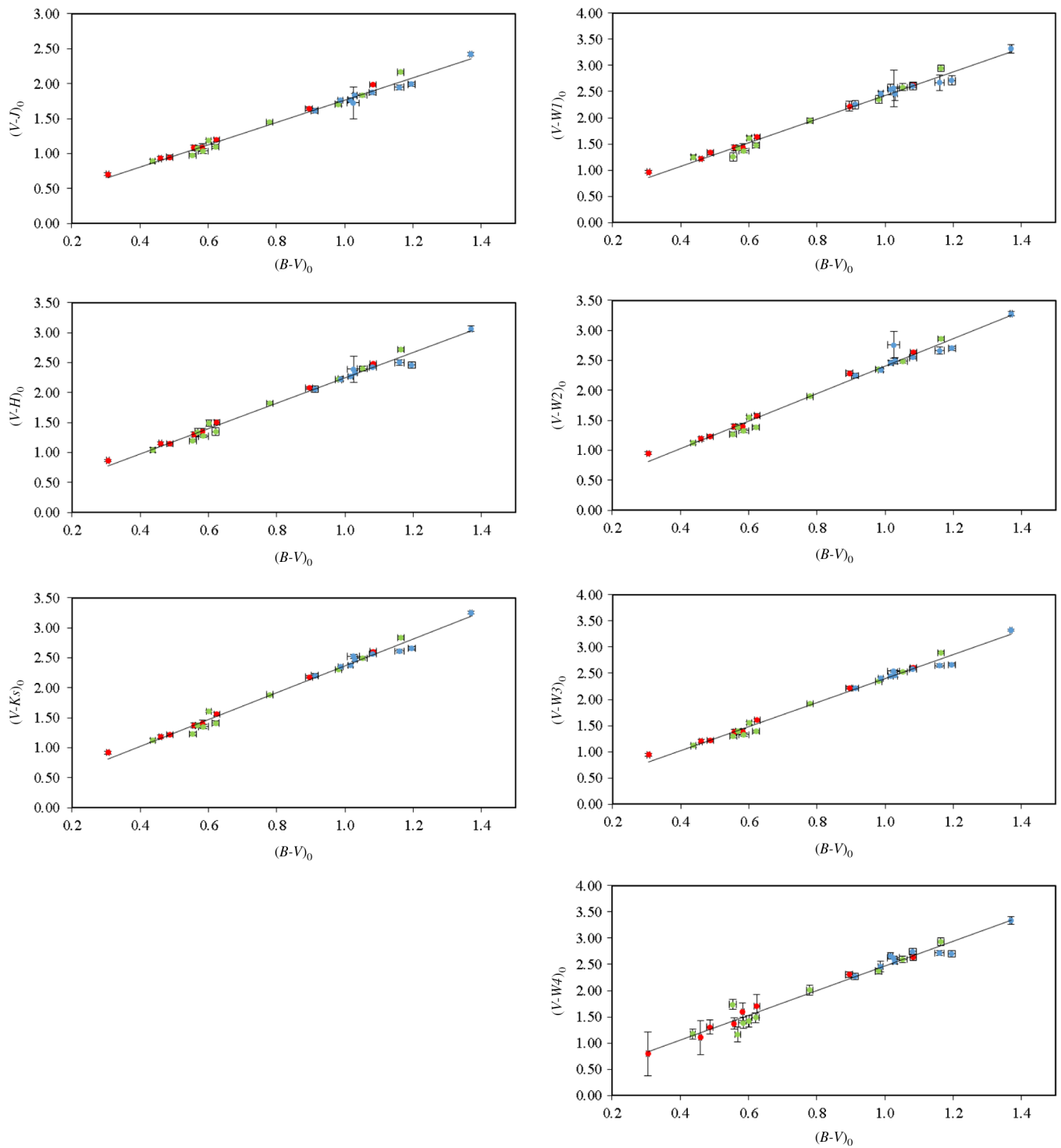
Figure A.1. Colour-colour graphs of the remaining seven linear-correlation fits (straight-lines) of reference stars, in $(V - \lambda)$. Giant (III) are indicated as blue, subgiants (IV) as green, and the main sequence stars (V) as red points. Colours are in magnitudes.
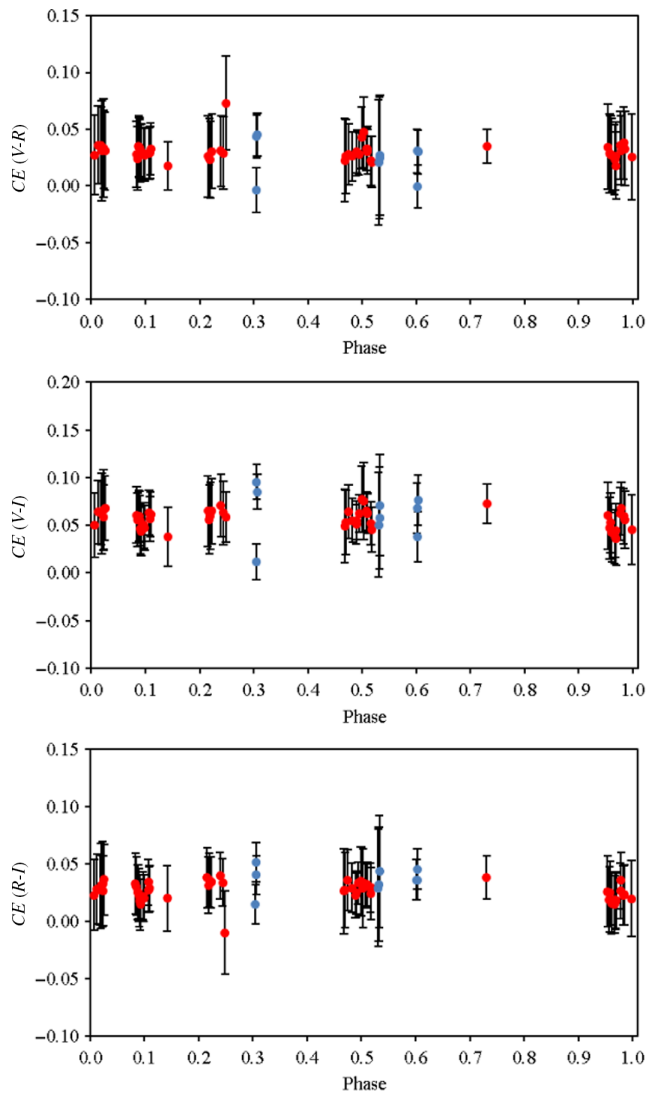
Figure A.2. The colour excesses of LX Per in $(V − R)$ (top panel), in $(V − I)$ (middle panel) and in (R-I) (bottom panel) as a function of orbital phase. Blue and red points are indicated as TUG's values and AUKR's values, respectively. CE values are in magnitudes. See text for explanation of relative error bars.
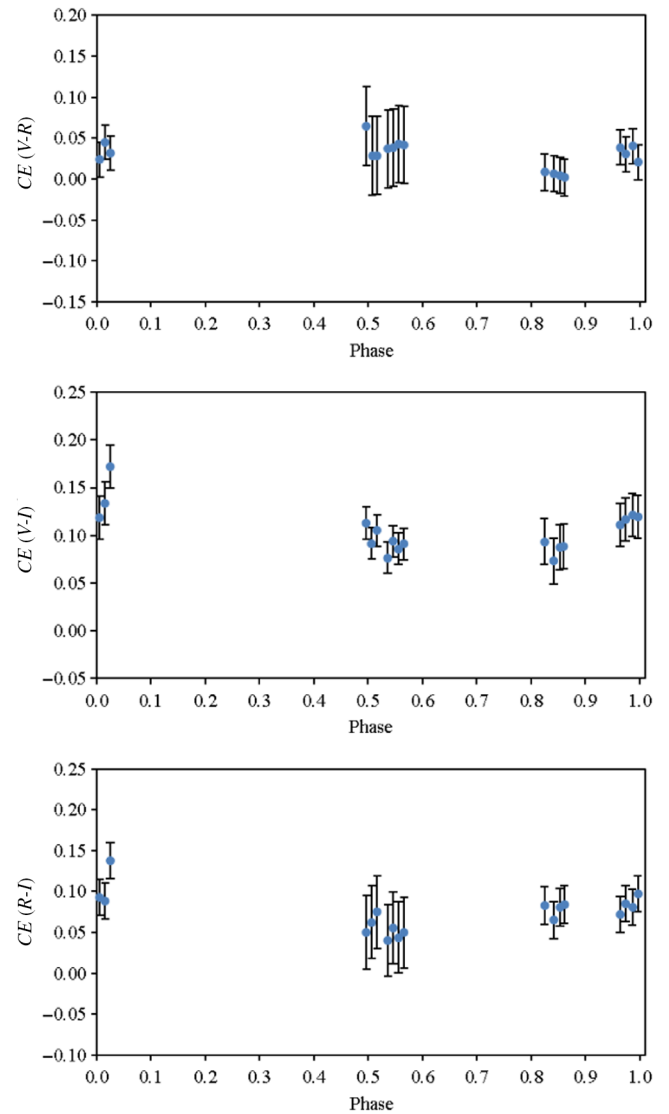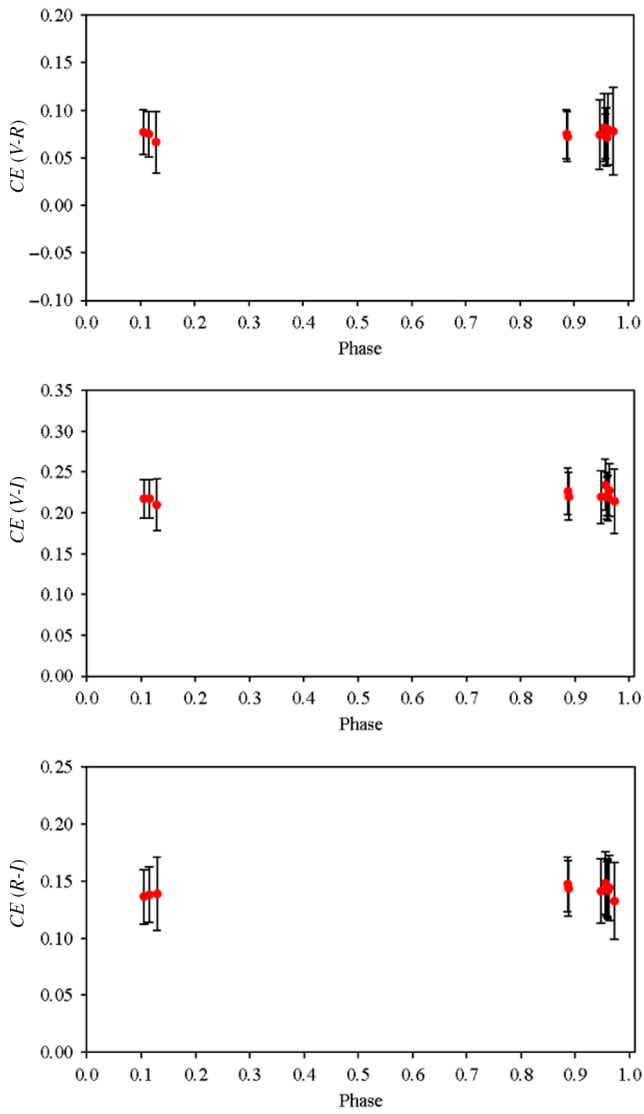
Figure A.3. Same as Figure A.2, but for SV Cam.

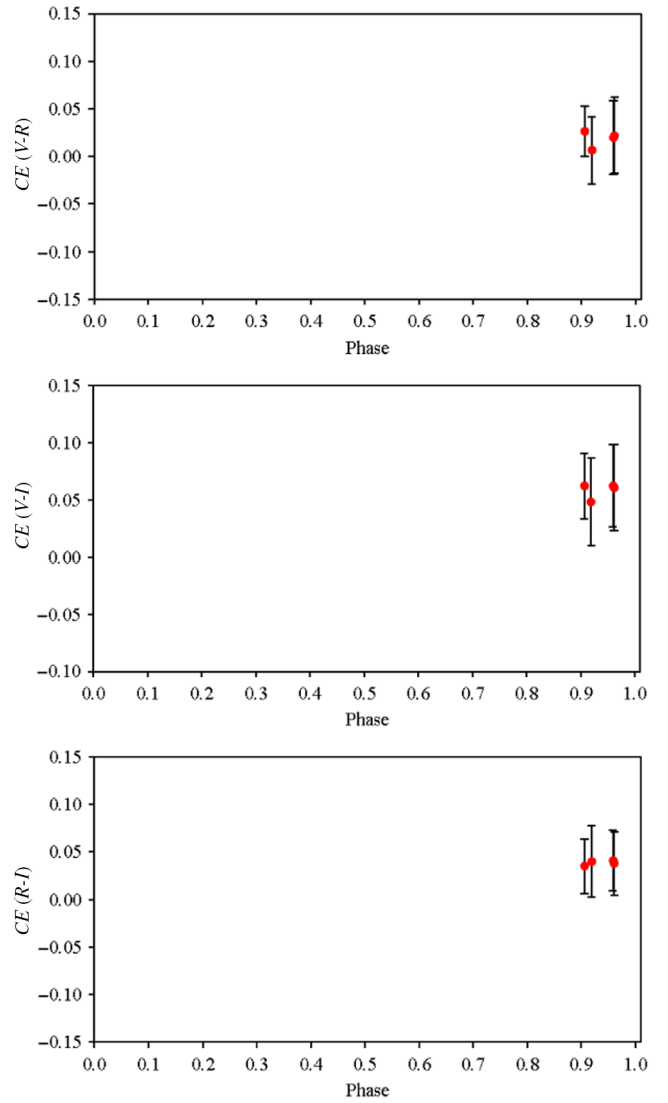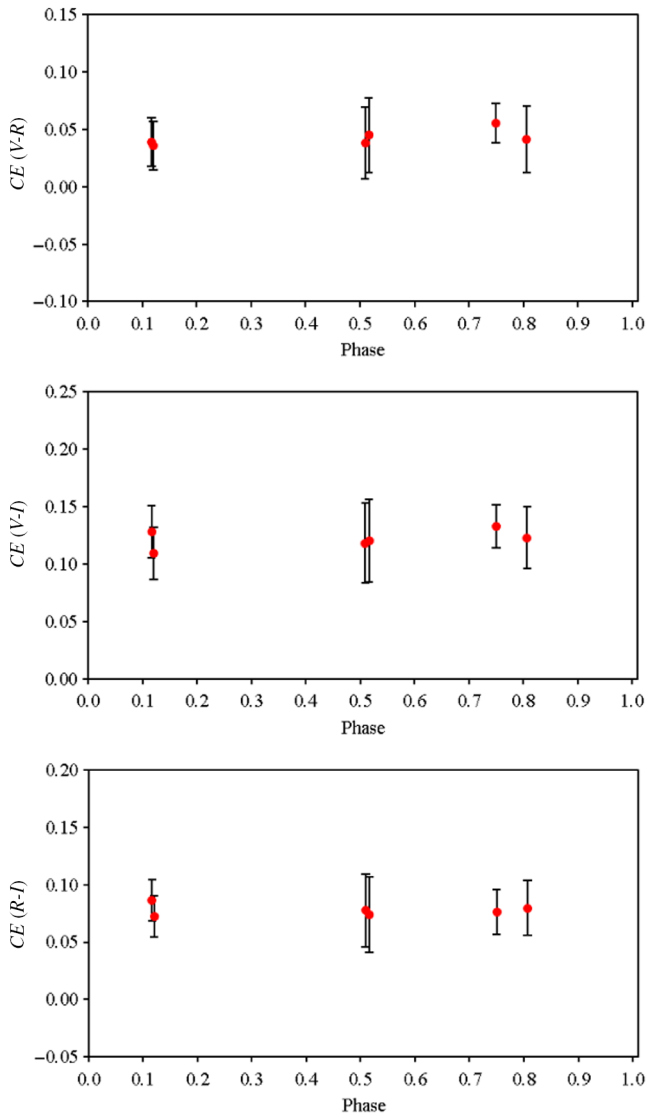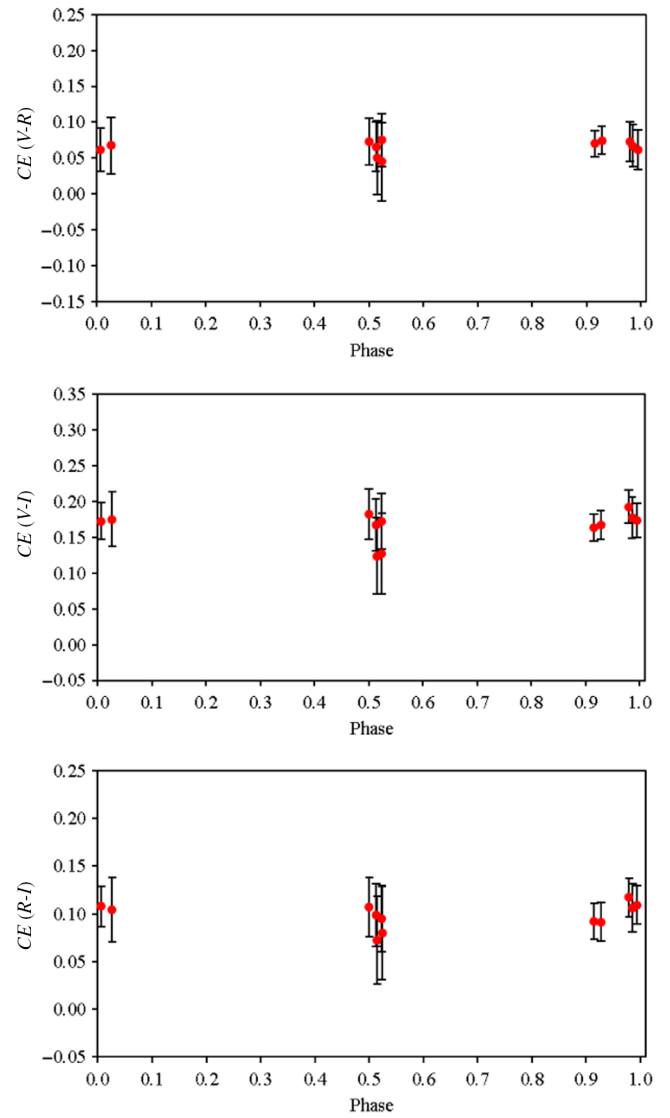**Figure A.4.** Same as Figure A.2, but for VV Mon.

Figure A.5. Same as Figure A.2, but for GK Hya.

Figure A.6. Same as Figure A.2, but for RW UMa.

Figure A.7. Same as Figure A.2, but for UX Com.

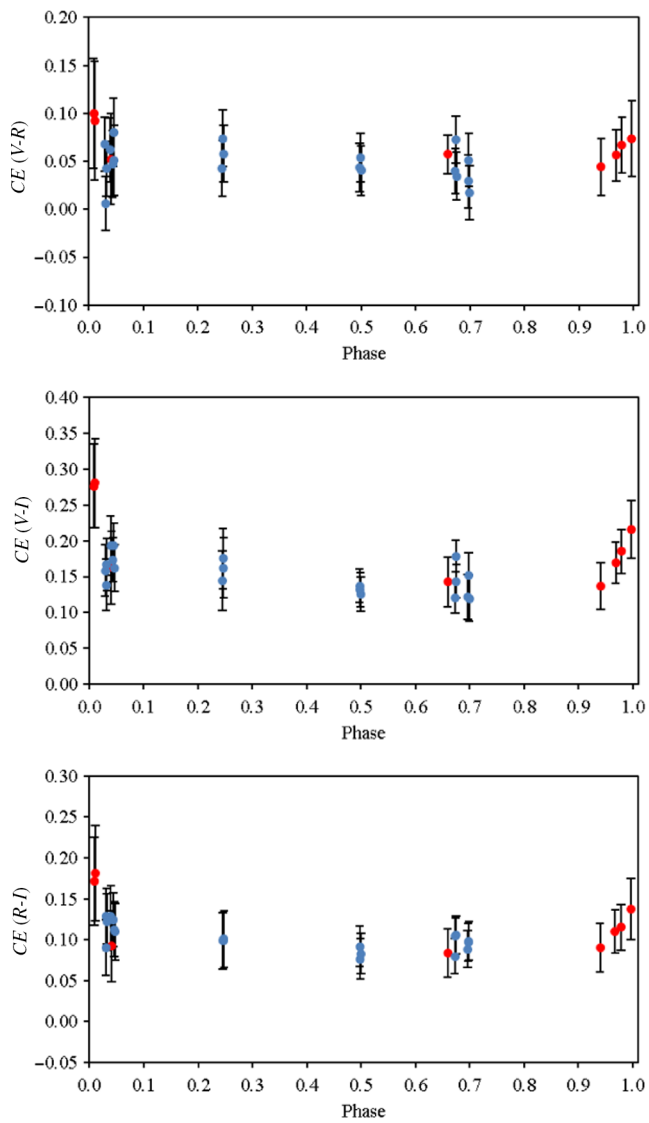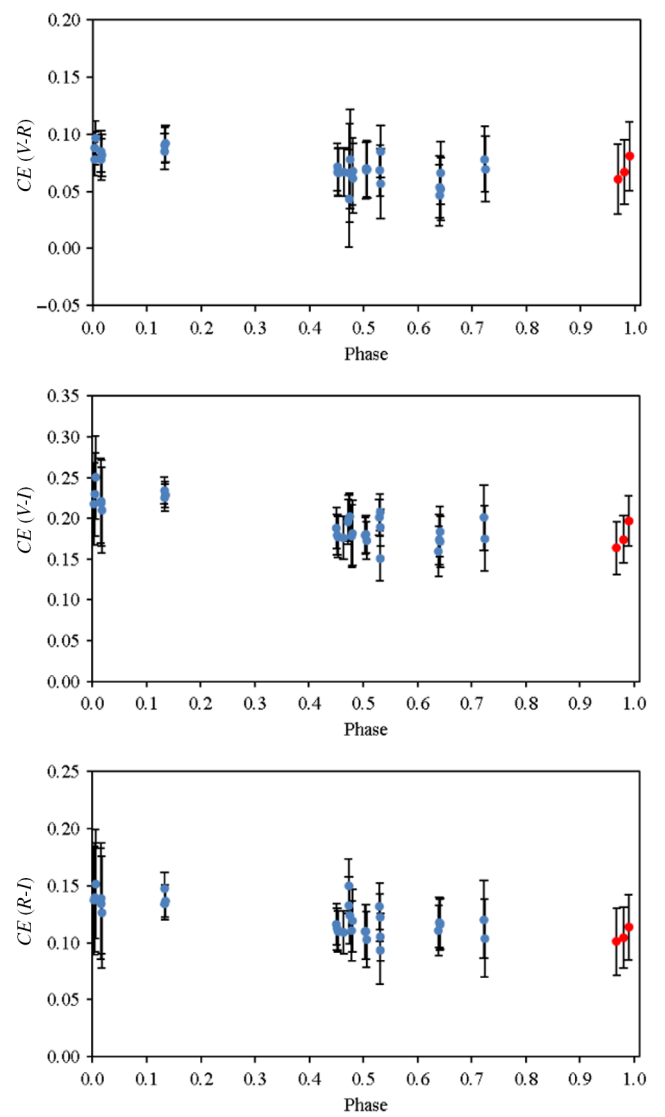**Figure A.8.** Same as Figure A.2, but for RS CVn.

Figure A.9. Same as Figure A.2, but for SS Boo.
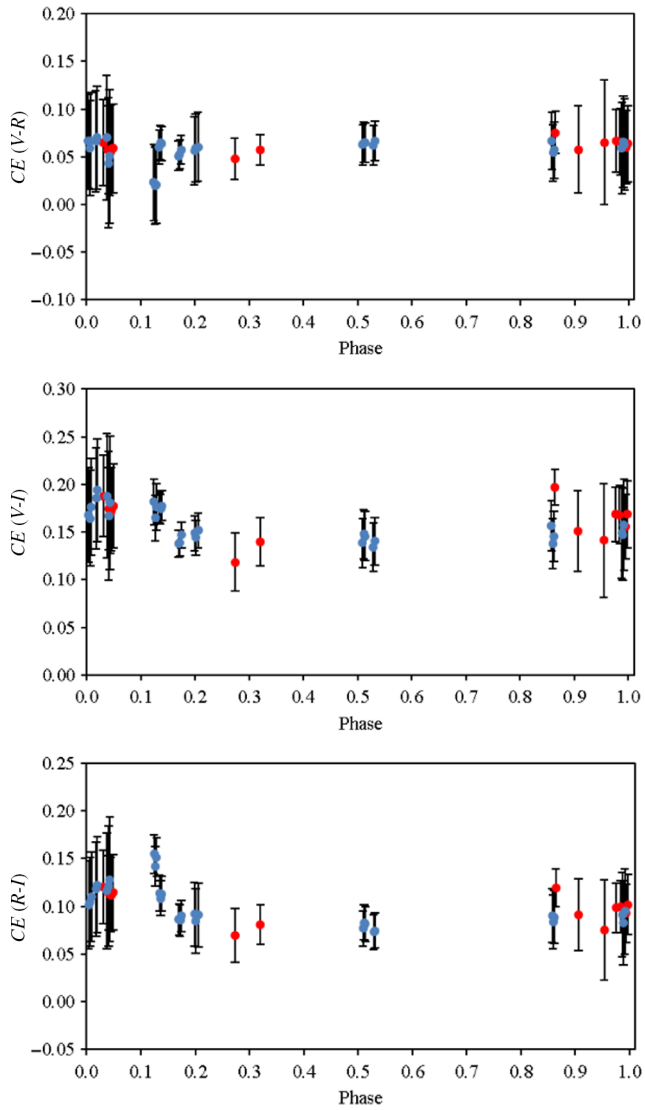
Figure A.10. Same as Figure A.2, but for PW Her.
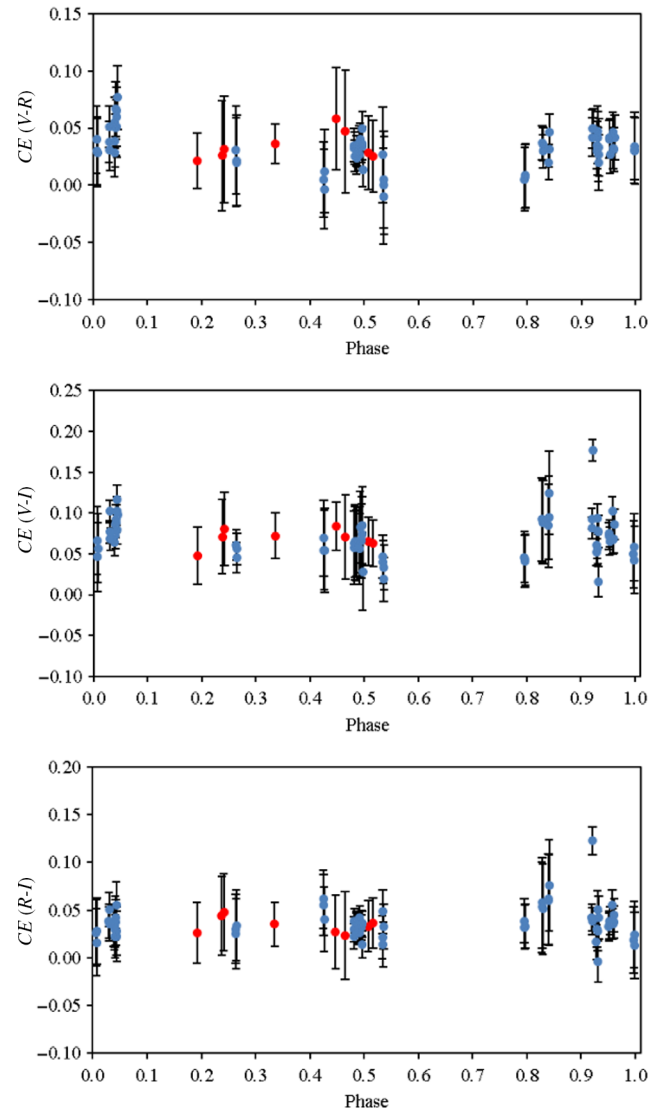
Figure A.11. Same as Figure A.2, but for AW Her.
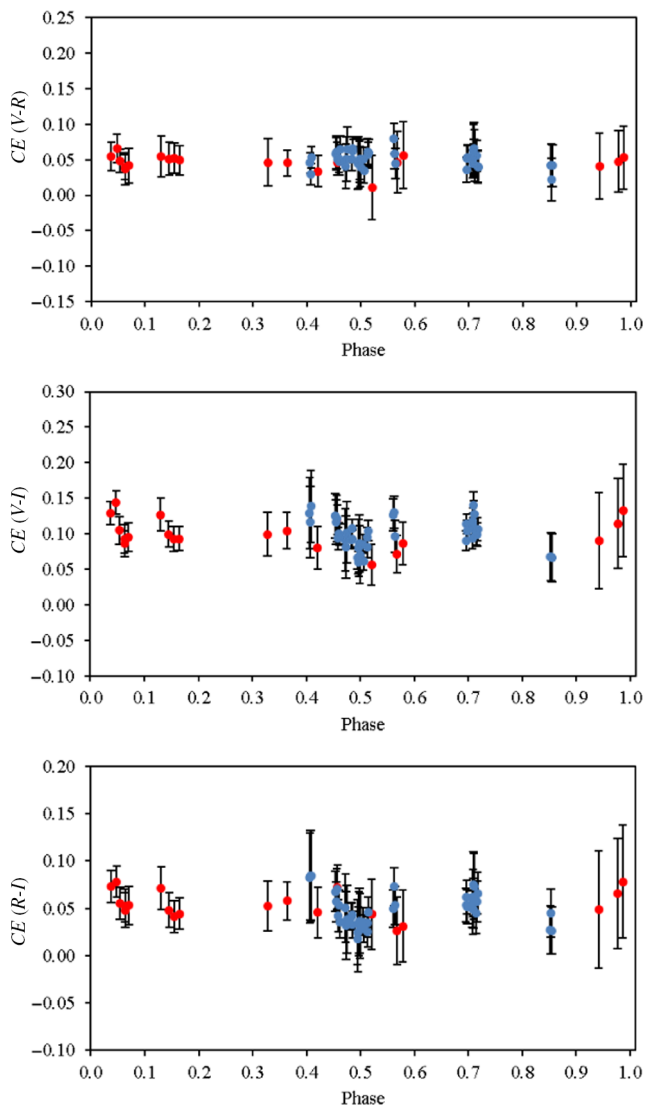
Figure A.12. Same as Figure A.2, but for RT Lac.
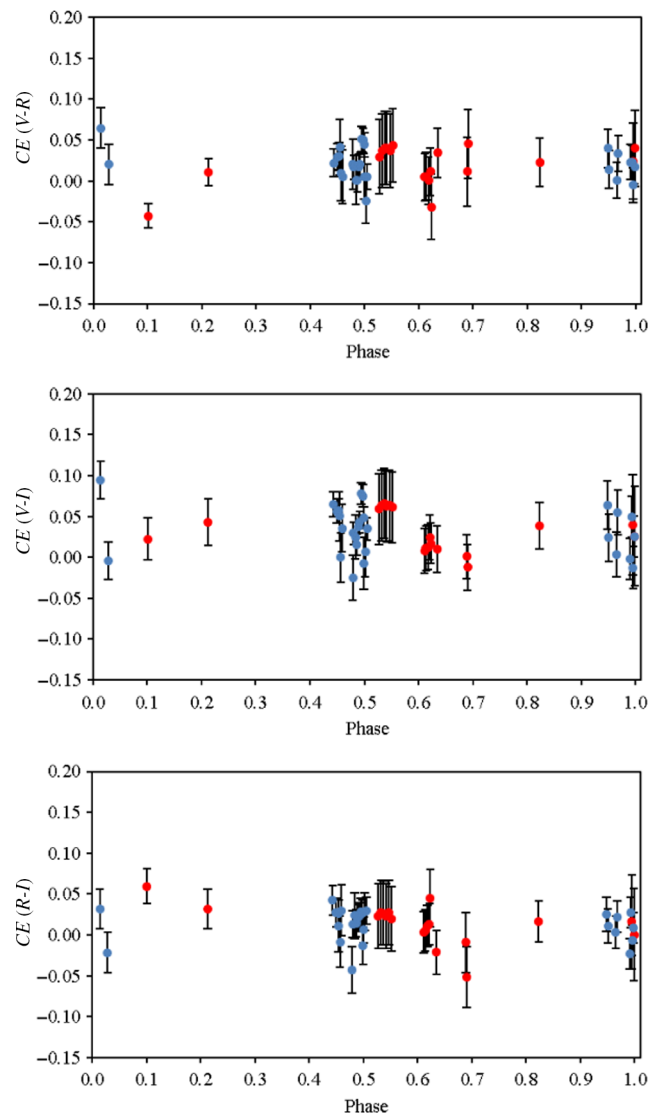
Figure A.13. Same as Figure A.2, but for AR Lac.
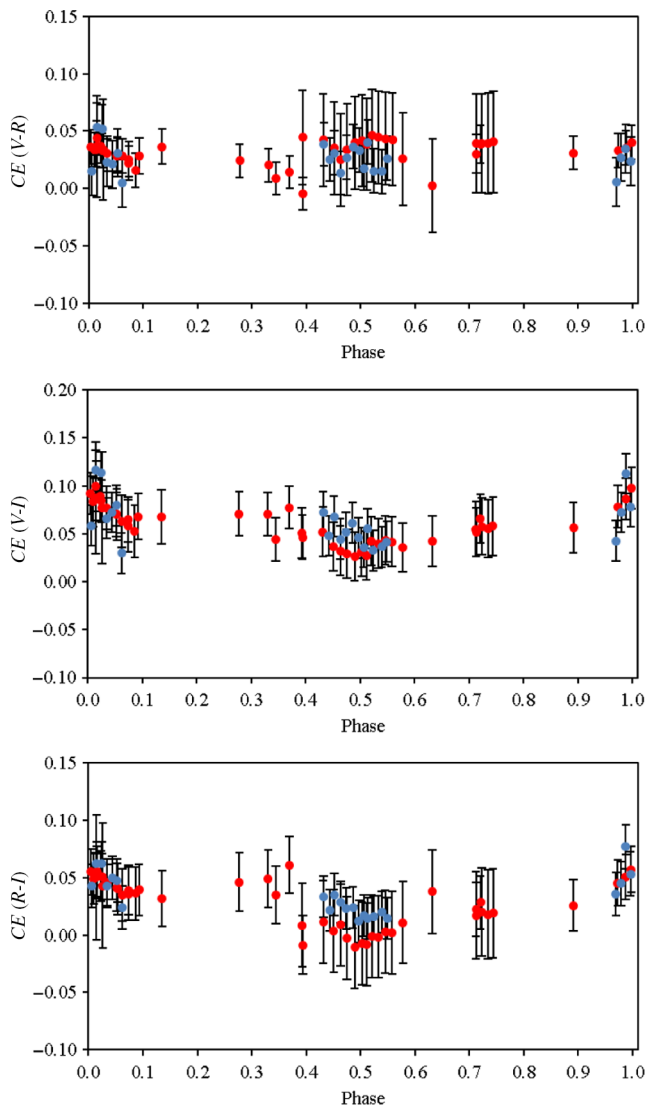
Figure A.14. Same as Figure A.2, but for RT And.
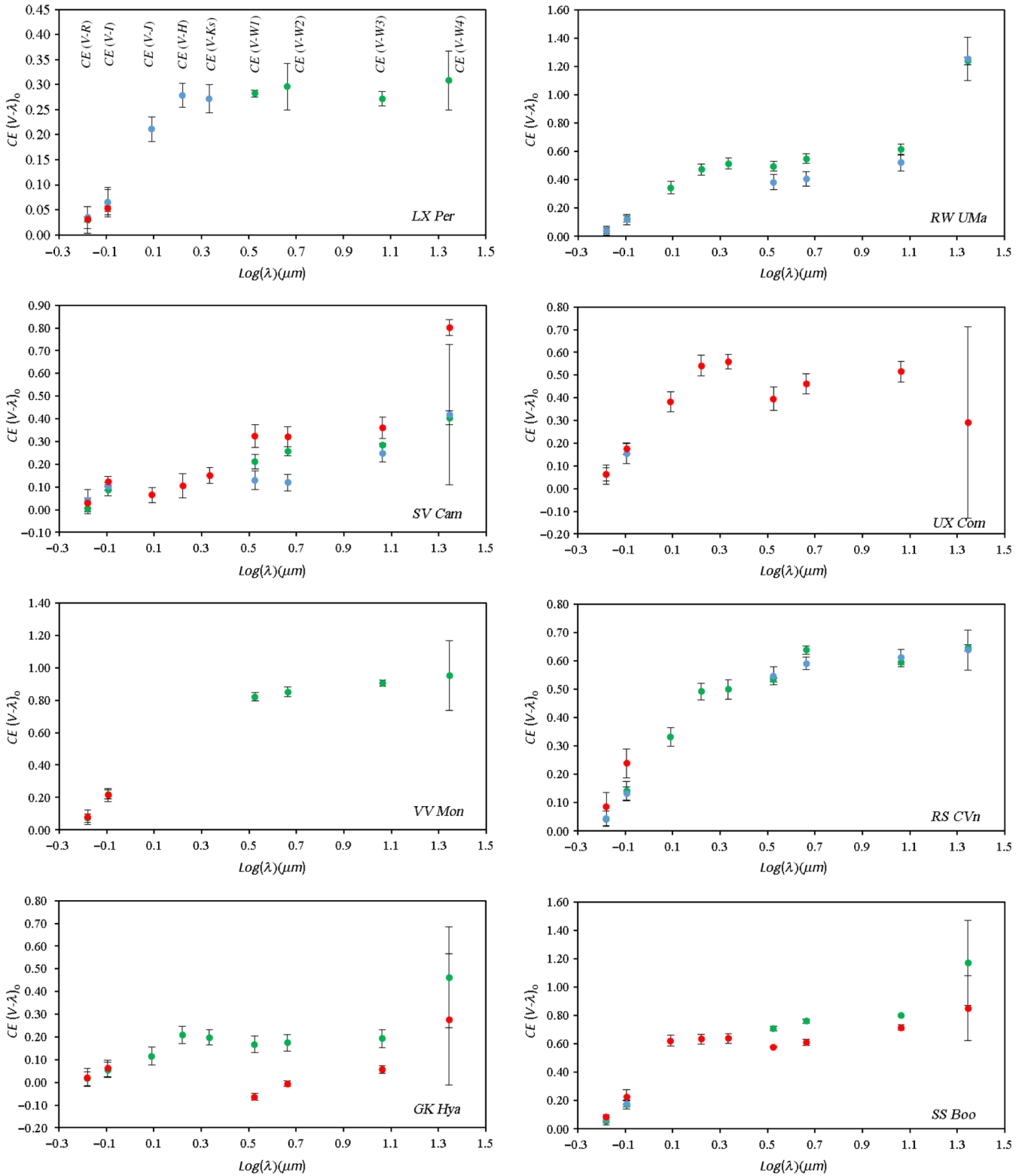
Figure A.15. As a function of wavelength, the colour excesses of 13 chromospherically active eclipsing binary systems in all bands during minima and outside eclipses (0.0P are indicated as red colour, 0.5P as blue, and the outside phases as green points). Although large errors of W4 data, the CE(V-W4) values are included in the plots to show only general tendencies. CE values are in magnitudes.

Figure A.15. Continued.

Figure A.16. Excess in $(V - \lambda)$ as a function of $(B - V)_o$ for 13 program stars; at the primary minima. Distributions of the excesses in $(V - W4)$ colours were not shown due to their large scatter.

Figure A.17. The evolutionary status of program stars (in red colours) and reference stars (in blue colours).

Table A.1: Photometric data of the reference stars. Colours are in units of magnitudes

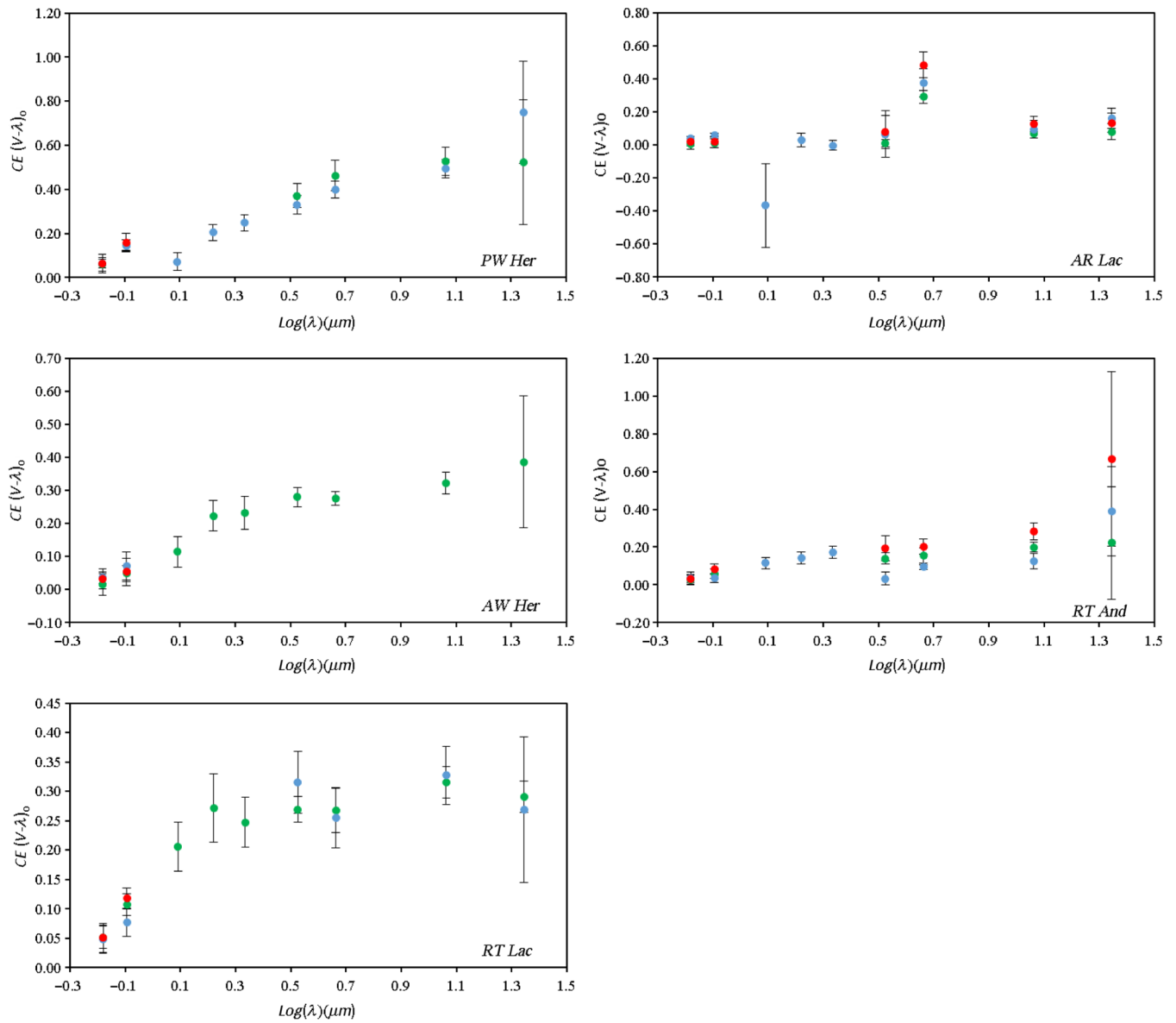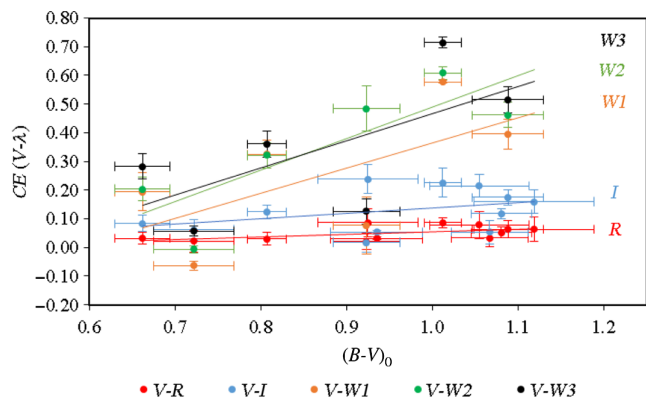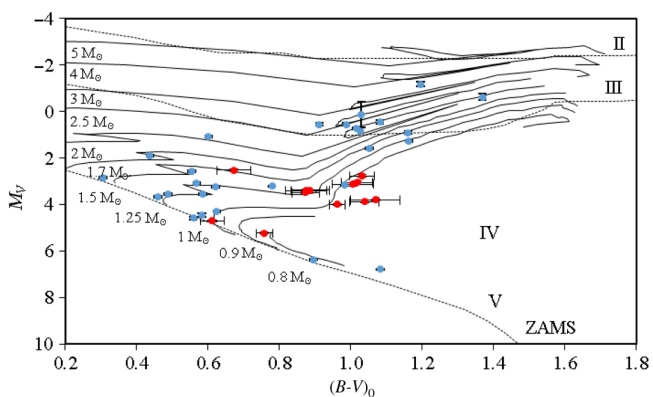| Star	π (mas) (Err)	$A_{(v)}d(b)$ (mag)	$(B-V)_o$ (Err)(mag)	$(V-R)_o$ (Err)(mag)	$(V-I)_o$ (Err)(mag)	$(R-I)_o$ (Err)(mag)	$(V-J)_o$ (Err)(mag)	$(V-H)_o$ (Err)(mag)	$(V-Ks)_o$ (Err)(mag)	$(B-V)_o$ (Err)(mag)	$(V-W1)_o$ (Err)(mag)	$(V-W2)_o$ (Err)(mag)	$(V-W3)_o$ (Err)(mag)	$(V-W4)_o$ (Err)(mag)
HD 116044	2.498 (0.028)	0.103	0.912 (0.009)	0.468 (0.003)	0.891 (0.009)	0.423 (0.008)	1.61 (0.03)	2.06 (0.05)	2.19 (0.03)	0.912 (0.009)	2.25 (0.09)	2.25 (0.04)	2.22 (0.03)	2.27 (0.06)
HD 232843	2.431 (0.545)	0.454	1.029 (0.007)	0.518 (0.005)	0.956 (0.006)	0.439 (0.003)	1.83 (0.03)	2.33 (0.04)	2.47 (0.03)	1.029 (0.007)	2.46 (0.13)	2.49 (0.06)	2.45 (0.03)	2.55 (0.05)
BD + 01 1945	1.637 (0.034)	0.072	0.987 (0.007)	0.489 (0.009)	0.956 (0.013)	0.465 (0.012)	1.76 (0.01)	2.23 (0.04)	2.35 (0.01)	0.987 (0.007)	2.46 (0.04)	2.34 (0.02)	2.39 (0.02)	2.46 (0.09)
HD 231848	3.008 (0.037)	0.22	1.016 (0.008)	0.509 (0.005)	0.954 (0.007)	0.446 (0.006)	1.77 (0.03)	2.27 (0.03)	2.37 (0.03)	1.016 (0.008)	2.54 (0.11)	2.46 (0.04)	2.45 (0.03)	2.66 (0.06)
HD 210925	7.323 (0.036)	0.086	1.025 (0.018)	0.544 (0.009)	1.036 (0.011)	0.493 (0.012)	1.72 (0.23)	2.39 (0.22)	2.53 (0.04)	1.025 (0.018)	2.56 (0.35)	2.76 (0.23)	2.54 (0.02)	2.63 (0.03)
HD 292944	1.726 (0.063)	0.266	1.081 (0.011)	0.529 (0.011)	1.001 (0.012)	0.472 (0.002)	1.87 (0.03)	2.43 (0.02)	2.57 (0.02)	1.081 (0.011)	2.61 (0.07)	2.55 (0.02)	2.58 (0.02)	2.75 (0.06)
HD 131447	3.13 (0.03)	0.054	1.159 (0.011)	0.593 (0.011)	1.084 (0.012)	0.494 (0.011)	1.95 (0.03)	2.49 (0.05)	2.61 (0.03)	1.159 (0.011)	2.67 (0.15)	2.66 (0.06)	2.65 (0.03)	2.72 (0.05)
HD 235751	0.959 (0.034)	0.476	1.195 (0.011)	0.559 (0.003)	1.048 (0.009)	0.489 (0.008)	1.99 (0.03)	2.46 (0.06)	2.66 (0.03)	1.195 (0.011)	2.71 (0.09)	2.69 (0.03)	2.67 (0.03)	2.71 (0.06)
BD + 28 2165	0.827 (0.046)	0.026	1.369 (0.002)	0.718 (0.003)	1.353 (0.004)	0.637 (0.005)	2.42 (0.02)	3.06 (0.05)	3.25 (0.02)	1.369 (0.002)	3.32 (0.08)	3.28 (0.03)	3.32 (0.02)	3.34 (0.07)
HD 127824	4.936 (0.031)	0.051	0.437 (0.007)	0.253 (0.005)	0.489 (0.007)	0.236 (0.005)	0.89 (0.03)	1.04 (0.04)	1.12 (0.03)	0.437 (0.007)	1.25 (0.05)	1.12 (0.03)	1.12 (0.03)	1.17 (0.09)
HD 336601	7.048 (0.058)	0.082	0.568 (0.008)	0.314 (0.011)	0.605 (0.005)	0.291 (0.009)	1.07 (0.04)	1.34 (0.06)	1.37 (0.04)	0.568 (0.008)	1.42 (0.05)	1.39 (0.04)	1.39 (0.04)	1.17 (0.14)
HD 195405	9.365 (0.033)	0.29	0.554 (0.011)	0.284 (0.006)	0.515 (0.009)	0.232 (0.005)	0.98 (0.02)	1.2 (0.02)	1.23 (0.03)	0.554 (0.011)	1.25 (0.08)	1.27 (0.03)	1.29 (0.04)	1.74 (0.09)
HD 18403	10.15 (0.045)	0.14	0.585 (0.014)	0.309 (0.006)	0.577 (0.008)	0.269 (0.002)	1.03 (0.04)	1.27 (0.03)	1.35 (0.03)	0.585 (0.014)	1.37 (0.04)	1.33 (0.03)	1.33 (0.03)	1.38 (0.11)
HD 291029	3.019 (0.038)	0.687	0.601 (0.007)	0.293 (0.004)	0.551 (0.007)	0.256 (0.004)	1.18 (0.02)	1.49 (0.06)	1.61 (0.02)	0.601 (0.007)	1.61 (0.04)	1.56 (0.03)	1.55 (0.03)	1.42 (0.11)
BD + 28 3198	8.565 (0.033)	0.101	0.621 (0.009)	0.333 (0.006)	0.62 (0.012)	0.286 (0.009)	1.11 (0.03)	1.35 (0.07)	1.41 (0.03)	0.621 (0.009)	1.48 (0.05)	1.39 (0.03)	1.39 (0.03)	1.48 (0.09)
BD + 26 3026	6.755 (0.029)	0.065	0.779 (0.009)	0.424 (0.008)	0.809 (0.008)	0.385 (0.008)	1.45 (0.02)	1.82 (0.02)	1.88 (0.02)	0.779 (0.009)	1.94 (0.05)	1.89 (0.02)	1.92 (0.02)	2.01 (0.11)
HD 111094	6.919 (0.032)	0.014	0.982 (0.009)	0.521 (0.007)	0.967 (0.009)	0.447 (0.004)	1.71 (0.03)	2.22 (0.02)	2.29 (0.02)	0.982 (0.009)	2.35 (0.08)	2.35 (0.03)	2.34 (0.02)	2.37 (0.06)
BD + 54 2777	2.879 (0.027)	0.232	1.051 (0.015)	0.539 (0.008)	1.014 (0.008)	0.477 (0.009)	1.84 (0.03)	2.39 (0.04)	2.49 (0.02)	1.051 (0.015)	2.58 (0.07)	2.48 (0.03)	2.53 (0.03)	2.59 (0.06)
TYC 3973-2446-1	1.939 (0.026)	0.156	1.163 (0.009)	0.615 (0.004)	1.175 (0.019)	0.559 (0.021)	2.16 (0.02)	2.72 (0.03)	2.84 (0.03)	1.163 (0.009)	2.95 (0.06)	2.86 (0.03)	2.89 (0.02)	2.93 (0.07)
BD + 46 1042	4.957 (0.046)	0.261	0.305 (0.004)	0.181 (0.006)	0.372 (0.007)	0.189 (0.004)	0.69 (0.02)	0.87 (0.02)	0.92 (0.02)	0.305 (0.004)	0.97 (0.03)	0.95 (0.02)	0.94 (0.03)	0.79 (0.42)
HD 95975	6.412 (0.029)	0.012	0.459 (0.004)	0.272 (0.002)	0.531 (0.008)	0.258 (0.006)	0.93 (0.02)	1.15 (0.03)	1.18 (0.03)	0.459 (0.004)	1.22 (0.03)	1.19 (0.03)	1.19 (0.03)	1.11 (0.32)
HD 216685	9.284 (0.044)	0.053	0.487 (0.009)	0.275 (0.005)	0.532 (0.007)	0.257 (0.006)	0.95 (0.03)	1.14 (0.03)	1.22 (0.03)	0.487 (0.009)	1.33 (0.04)	1.23 (0.03)	1.22 (0.03)	1.29 (0.13)
HD 145404	16.699 (0.033)	0.055	0.558 (0.004)	0.314 (0.009)	0.605 (0.013)	0.291 (0.006)	1.08 (0.04)	1.29 (0.04)	1.37 (0.04)	0.558 (0.004)	1.43 (0.05)	1.39 (0.04)	1.38 (0.04)	1.37 (0.11)
HD 259516	11.384 (0.064)	0.067	0.583 (0.004)	0.321 (0.004)	0.624 (0.005)	0.302 (0.001)	1.08 (0.06)	1.35 (0.06)	1.41 (0.06)	0.583 (0.004)	1.44 (0.06)	1.39 (0.06)	1.38 (0.06)	1.59 (0.17)
HD 111540	8.854 (0.079)	0.017	0.624 (0.009)	0.347 (0.002)	0.669 (0.004)	0.322 (0.005)	1.19 (0.03)	1.49 (0.04)	1.56 (0.03)	0.624 (0.009)	1.63 (0.03)	1.58 (0.03)	1.59 (0.03)	1.71 (0.23)
HD 56168	38.658 (0.038)	0.012	0.895 (0.011)	0.512 (0.011)	0.942 (0.011)	0.432 (0.002)	1.64 (0.02)	2.08 (0.03)	2.18 (0.02)	0.895 (0.011)	2.22 (0.09)	2.29 (0.04)	2.22 (0.03)	2.31 (0.05)
HD 233357	36.966 (0.045)	0.019	1.082 (0.009)	0.643 (0.002)	1.149 (0.007)	0.512 (0.009)	1.98 (0.02)	2.48 (0.02)	2.59 (0.02)	1.082 (0.009)	2.62 (0.05)	2.63 (0.03)	2.61 (0.02)	2.63 (0.05)

Table A.2: Colour excess *CE* values of program stars

Star	Min. Type	$(B−V)_o$(Err) (mag)	CE in $(V−R)$(Err) (mag)	CE in $(V−I)$(Err) (mag)	CE in $(R−I)$(Err) (mag)	CE in $(V−J)$(Err) (mag)	CE in $(V−H)$(Err) (mag)	CE in $(V−Ks)$(Err) (mag)	$(B−V)_o$(Err) (mag)	CE in $(V−W1)$(Err) (mag)	CE in $(V−W2)$(Err) (mag)	CE in $(V−W3)$(Err) (mag)	CE in $(V−W4)$(Err) (mag)
	I	0.885 (0.054)	0.031 (0.005)	−0.053 (0.005)	0.022 (0.001)		−	−	0.885 (0.054)	−	−	−	−
LX Per	II	0.682 (0.038)	0.035 (0.022)	0.066 (0.025)	0.031 (0.023)	0.21 (0.02)	0.28 (0.02)	0.27 (0.03)	0.682 (0.038)	−	−	−	−
	Outside	0.706 (0.035)	0.029 (0.027)	− 0.065 (0.029)	0.035 (0.021)		−	−	0.706 (0.035)	0.28 (0.01)	0.31 (0.05)	0.27 (0.01)	0.31 (0.06)
	I	0.757 (0.023)	0.030 (0.021)	0.124 (0.023)	0.093 (0.022)	0.07 (0.03)	0.11 (0.05)	0.15 (0.03)	0.757 (0.023)	0.32 (0.05)	0.32 (0.04)	0.36 (0.05)	0.81 (0.04)
SV Cam	II	0.691 (0.029)	0.041 (0.048)	− 0.103 (0.017)	0.062 (0.045)		−	−	0.691 (0.029)	0.13 (0.04)	0.12 (0.04)	0.25 (0.04)	0.42 (0.31)
	Outside	0.681 (0.024)	0.005 (0.022)	− 0.086 (0.024)	0.078 (0.023)		−	−	0.681 (0.024)	0.21 (0.03)	0.26 (0.02)	0.28 (0.01)	0.04 (0.03)
	I	1.005 (0.058)	0.078 (0.046)	− 0.214 (0.039)	0.133 (0.034)		−	−	1.005 (0.058)	−	−	−	−
VV Mon	II	−	−	−	−	−	−	−	−	−	−	−	−
	Outside	0.778 (0.039)	0.072 (0.027)	− 0.218 (0.028)	0.142 (0.026)		−	−	0.778 (0.039)	0.82 (0.03)	0.85 (0.03)	0.91 (0.02)	0.95 (0.21)
	I	0.672 (0.047)	0.021 (0.039)	− 0.062 (0.037)	0.041 (0.033)		−	−	0.672 (0.047)	−0.06 (0.02)	−0.01 (0.01)	0.06 (0.02)	0.28(0.29)
GK Hya	II	−	−	−	−	−	−	−	−	−	−	−	−
	Outside	0.678 (0.045)	0.017 (0.031)	0.055 (0.033)	0.038 (0.033)	0.12 (0.04)	0.21 (0.04)	0.20 (0.03)	0.678 (0.045)	0.17 (0.04)	0.17 (0.04)	0.19 (0.04)	0.46 (0.22)
	I	−	−	−	−		−	−	−	−	−	−	−
RW UMa	II	0.615 (0.047)	0.042 (0.032)	− 0.119 (0.035)	0.076 (0.032)		−	−	0.615 (0.047)	0.38 (0.05)	0.41 (0.05)	0.52 (0.06)	1.25 (0.15)
	Outside	0.643 (0.028)	0.043 (0.022)	0.123 (0.023)	0.079 (0.020)	0.35 (0.04)	0.47 (0.04)	0.52 (0.04)	0.643 (0.028)	0.49 (0.03)	0.55 (0.03)	0.61 (0.04)	1.24 (0.03)
	I	1.038 (0.041)	0.064 (0.029)	0.175 (0.026)	0.108 (0.022)	0.38 (0.04)	0.54 (0.05)	0.56 (0.03)	1.038 (0.041)	0.40 (0.05)	0.46 (0.04)	0.51 (0.05)	0.29 (0.42)
UX Com	II	0.851 (0.061)	0.062 (0.042)	− 0.155 (0.044)	0.091 (0.039)		−	−	0.851 (0.061)	−	−	−	−
	Outside	−	−	−	−	−	−	−	−	−	−	−	−
	I	0.875 (0.058)	0.087 (0.049)	− 0.239 (0.052)	0.148 (0.049)		−	−	0.875 (0.058)	−	−	−	−
RS CVn	II	0.587 (0.027)	0.046 (0.026)	− 0.132 (0.024)	0.084 (0.025)		−	−	0.587 (0.027)	0.55 (0.03)	0.59 (0.02)	0.61 (0.03)	0.64 (0.07)
	Outside	0.622 (0.033)	0.043 (0.027)	0.142 (0.032)	0.096 (0.026)	0.33 (0.03)	0.49 (0.03)	0.51 (0.03)	0.622 (0.033)	0.53 (0.01)	0.64 (0.01)	0.59 (0.02)	0.65 (0.01)

Table A.2: Continued

Star	Min. Type	$(B-V)_o$(Err) (mag)	CE in $(V-R)$(Err) (mag)	CE in $(V-I)$(Err) (mag)	CE in $(R-I)$(Err) (mag)	CE in $(V-J)$(Err) (mag)	CE in $(V-H)$(Err) (mag)	CE in $(V-Ks)$(Err) (mag)	$(B-V)_o$(Err) (mag)	CE in $(V-W1)$(Err) (mag)	CE in $(V-W2)$(Err) (mag)	CE in $(V-W3)$(Err) (mag)	CE in $(V-W4)$(Err) (mag)
	I	0.962 (0.021)	0.086 (0.017)	0.226 (0.052)	0.138 (0.048)	0.62 (0.04)	0.63 (0.03)	0.64 (0.03)	0.962 (0.021)	0.58 (0.01)	0.61 (0.02)	0.71 (0.02)	0.85 (0.23)
SS Boo	II	0.781 (0.025)	0.069 (0.025)	− 0.177 (0.023)	0.107 (0.024)		−	−	0.781 (0.025)	−	−	−	−
	Outside	0.797 (0.023)	0.055 (0.027)	− 0.173 (0.031)	0.115 (0.022)		−	−	0.797 (0.023)	0.71 (0.02)	0.76 (0.01)	0.80 (0.01)	1.17 (0.30)
	I	1.069 (0.071)	0.064 (0.044)	− 0.159 (0.042)	0.095 (0.038)		−	−	1.069 (0.071)	−	−	−	−
PW Her	II	0.859 (0.031)	0.064 (0.021)	0.144 (0.026)	0.081 (0.019)	0.07 (0.04)	0.21 (0.04)	0.25 (0.04)	0.859 (0.031)	0.33 (0.04)	0.39 (0.04)	0.49 (0.04)	0.75 (0.23)
	Outside	0.871 (0.026)	0.060 (0.032)	− 0.147 (0.023)	0.088 (0.031)		−	−	0.871 (0.026)	0.37 (0.05)	0.46 (0.07)	0.53 (0.06)	0.52 (0.28)
	I	1.017 (0.045)	0.032 (0.029)	− 0.053 (0.041)	0.021 (0.035)		−	−	1.017 (0.045)	−	−	−	−
AW Her	II	0.719 (0.023)	0.036 (0.017)	− 0.071 (0.043)	0.033 (0.015)		−	−	0.719 (0.023)	−	−	−	−
	Outside	0.769 (0.022)	0.016 (0.033)	0.049 (0.025)	0.032 (0.031)	0.11 (0.05)	0.22 (0.05)	0.23 (0.05)	0.769 (0.022)	0.28 (0.03)	0.28 (0.02)	0.32 (0.03)	0.39 (0.20)
	I	1.031 (0.035)	0.052 (0.019)	− 0.118 (0.018)	0.065 (0.017)		−	−	1.031 (0.035)	−	−	−	−
RT Lac	II	1.112 (0.031)	0.048 (0.024)	− 0.078 (0.024)	0.031 (0.025)		−	−	1.112 (0.031)	0.31 (0.05)	0.25 (0.05)	0.33 (0.05)	0.27 (0.12)
	Outside	1.024 (0.028)	0.051 (0.024)	0.107 (0.018)	0.056 (0.022)	0.21 (0.04)	0.27 (0.06)	0.25 (0.04)	1.024 (0.028)	0.27 (0.02)	0.27 (0.04)	0.31 (0.03)	0.29 (0.03)
	I	0.873 (0.039)	0.020 (0.029)	− 0.017 (0.035)	0.010 (0.030)		−	−	0.873 (0.039)	0.08 (0.10)	0.48 (0.08)	0.13 (0.05)	0.13 (0.06)
AR Lac	II	0.739 (0.026)	0.037 (0.015)	− 0.059 (0.014)	0.023 (0.016)	0.37 (0.25)	0.03 (0.04)	0.01 (0.03)	0.739 (0.026)	0.07 (0.14)	0.38 (0.09)	0.09 (0.06)	0.16 (0.06)
	Outside	0.774 (0.042)	0.007 (0.032)	− 0.011 (0.027)	0.005 (0.028)		−	−	0.774 (0.042)	0.01 (0.02)	0.29 (0.04)	0.07 (0.03)	0.08 (0.05)
	I	0.612 (0.032)	0.031 (0.021)	− 0.083 (0.027)	0.051 (0.025)		−	−	0.612 (0.032)	0.19 (0.07)	0.21 (0.04)	0.28 (0.04)	0.67 (0.46)
RT And	II	0.505 (0.031)	0.037 (0.031)	0.038 (0.024)	0.002 (0.028)	0.12 (0.03)	0.14 (0.03)	0.17 (0.03)	0.505 (0.031)	0.03 (0.03)	0.09 (0.01)	0.12 (0.04)	0.39 (0.24)
	Outside	0.552 (0.038)	0.028 (0.027)	− 0.059 (0.026)	0.026 (0.030)		−	−	0.552 (0.038)	0.14 (0.03)	0.16 (0.04)	0.19 (0.02)	0.22 (0.31)

Table A.3: Summary of excess radiation results of the program stars during primary minimum

Star	π (mas)(*Err*)	$A_{(v)}d(b)$ (mag)	M_V (*Err*) (mag)	Optical Exc. (mag)	Near-IR Exc. (mag)	Middle-IR Exc. (mag)
LX Per	8.7 (0.039)	0.141	3.385 (0.015)	*in low level of* ∼0.04	*No observation*	*No observation*
SV Cam	11.777 (0.04)	0.039	5.229 (0.038)	*in level of* ∼0.09	∼0.1	∼0.3
VV Mon	3.579 (0.045)	0.002	3.125 (0.073)	*in level of* ∼0.15	*No observation*	*No observation*
GK Hya	4.275 (0.043)	0.073	2.524 (0.063)	*in low level of* ∼0.05	*No observation*	∼−0.04
RW Uma	2.666 (0.048)	0.041	*No observation*	*No observation*	*No observation*	*No observation*
UX Com	4.722 (0.045)	0.026	3.880 (0.057)	*in level of* ∼0.1	∼0.5	∼0.5
RS CVn	7.361 (0.041)	0.018	3.400 (0.060)	*in level of* ∼0.15	*No observation*	*No observation*
SS Boo	4.216 (0.026)	0.047	3.997 (0.046)	*in level of* ∼0.15	∼0.63	∼0.63
PW Her	4.378 (0.022)	0.080	3.798 (0.051)	*in level of* ∼0.1	*No observation*	*No observation*
AW Her	3.828 (0.051)	0.225	3.049 (0.079)	*in low level of* ∼0.04	*No observation*	*No observation*
RT Lac	5.488 (0.037)	0.200	2.764 (0.046)	*in level of* ∼0.08	*No observation*	*No observation*
AR Lac	23.433 (0.03)	0.045	3.485 (0.039)	in very low level of ∼0.02	*No observation*	∼0.2
RT And	10.127 (0.042)	0.072	4.695 (0.040)	*in low level of* ∼0.06	*No observation*	∼0.22